Highlights from BNL and RHIC 2014

M. J. Tannenbaum *
Physics Department, 510c,
Brookhaven National Laboratory,
Upton, NY 11973-5000, USA
mjt@bnl.gov

1 Introduction

The Relativistic Heavy Ion Collider (RHIC) at Brookhaven National Laboratory (BNL) is one of the two remaining operating hadron colliders, the other being the LHC at CERN. Unlike the LHC, which is buried in a deep underground tunnel, RHIC is built in an enclosure on the surface which is covered by an earth berm for shielding which can be seen from outer space (Fig. 1).

Figure 1: NASA infra-red photo of Long Island and the New York Metro Region from space. RHIC is the white circle to the left of the word BNL. Manhattan Island in New York City, ∼100 km west of BNL, is also clearly visible on the left side of the photo.

*Research supported by U. S. Department of Energy, DE-AC02-98CH10886.

BNL is a multipurpose laboratory, quite different in scope from Fermilab and CERN, with many "cutting edge" major research facilities in addition to RHIC. Figure 2 shows the two newest facilities: the National Synchrotron Light Source II (NSLS II) to come on-line October 1, 2014; and the Long Island Solar Farm which has an experimental section as well as supplying 32MW peak power to nearby homes in partnership with the local electric company.

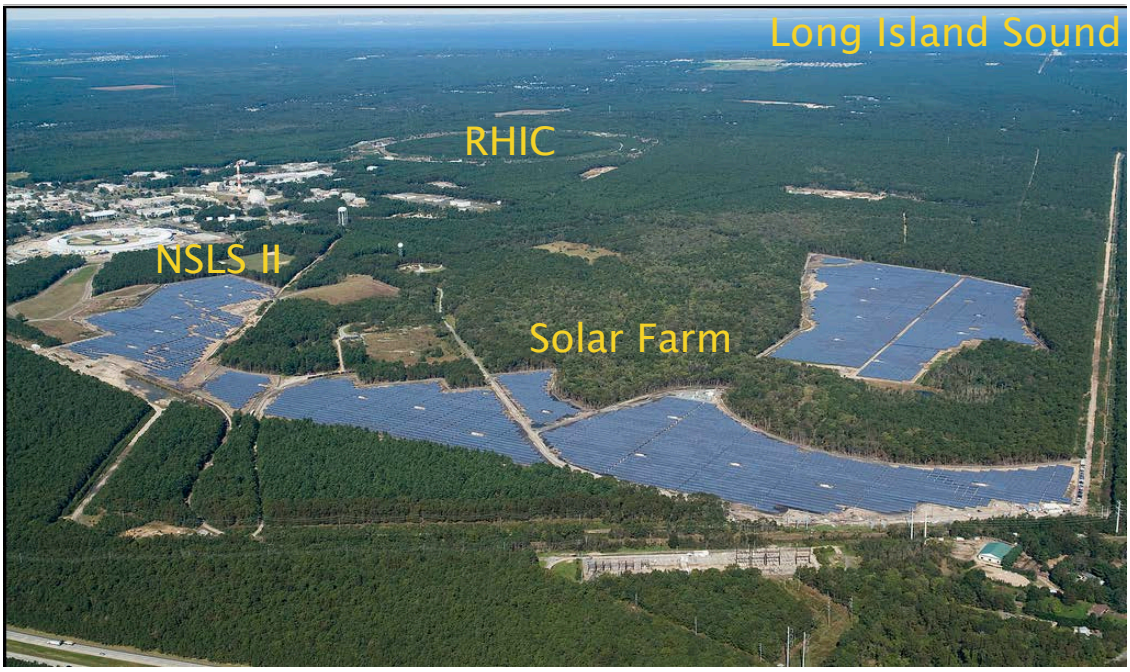

Figure 2: Aerial view of BNL with NSLS II, RHIC and the Solar Farm indicated.

2 News from BNL since ISSP2013

Although Fiscal Year 2014 started on October 1, 2013 with the U. S. Government shut down for the first 16 days due to the lack of an approved budget, the rest of the FY2014 turned out very well for BNL and RHIC. At the administrative level, Professor Robert Tribble of Texas A&M University, well known for both his physics research and leadership of two important U. S. Department of Energy (DoE) Panels in 2005 and 2013, was appointed Deputy Director for Science & Technology, effective February 2014. Not long after that, in March, the DoE issued a Request For Proposals for a "management and operating (M&O) contractor" for BNL, which is owned by the U.S. Government, but run by an M&O contractor. The present contractor, BSA, is a partnership of Battelle Memorial Institute, a private non-profit science and technology development company, headquartered in Columbus, Ohio, and Stony Brook University. BSA has been the M&O contractor at BNL for the past 15 years (out of the BNL's 67 year existence), with the "engagement" of six of the world's leading research universities (Columbia, Cornell, Harvard, MIT, Princeton and Yale) who were among the universities that formed the founding M&O contractor, Associated Universities Incorporated, along with Johns Hopkins, and the Universities of Pennsylvania and Rochester. The new contract starts on January 1, 2015, preceded by a maximum 2 month transition phase-in period so should be awarded near or soon after November 1, 2014 [1].

The U. S. High Energy Physics bureaucracy was not idle during this period, with the release of the "Particle Physics Project Prioritization Panel (P5)" Report to the High energy Physics Advisory Panel (HEPAP) on May 21, 2014. The charge of the panel was "to develop an updated strategic plan for U.S. high energy physics that can be executed over a 10 year timescale, in the context of a 20 year global vision for the field." Their reasonable top priority for constrained budget scenarios was to "Use the Higgs boson as a new tool for discovery" which is good news for the U. S. HEP groups working at the LHC at CERN; but lots of internal U. S. activities were "redirected" [2]. For the unconstrained budget scenario, all they could come up with was:

- Develop a greatly expanded accelerator R&D program that would emphasize the ability to build very high-energy accelerators beyond the High-Luminosity LHC (HL-LHC) and ILC at dramatically lower cost.
- Play a world-leading role in the ILC experimental program and provide critical expertise and components to the accelerator, *should this exciting scientific opportunity be realized in Japan.*

which IMHO lacks the imagination and drive of previous generations of U.S High Energy Physicists who had proposed and were constructing a 40 TeV p+p collider for completion in 1995 if not for ... [3].

Not to be outdone, the new Long Range Planning exercise for U. S. Nuclear Physics was initiated in April 2014.

3 RHIC Operations and accelerator future plans

Since beginning operation in the year 2000, RHIC, which can collide any species with any other species including polarized protons, has provided collisions at 14 different values of nucleon-nucleon c.m. energy, $\sqrt{s_{NN}}$, and ten different species combinations including Au+Au, d+Au, Cu+Cu, Cu+Au, U+U, and in 2014 He^3+Au, if differently polarized protons are counted as different species. The performance history of RHIC with A+A and

RHIC Run	Year	Species	Energy	Ldt
Run-1	2000	Au+Au	130 GeV	1 μb-1
Run-2	2001-2	Au+Au	200 GeV	24 μb-1
Run-2		Au+Au	19 GeV	0.4 μb-1
		p+p	200 Gev	150 nb-1
Run-3	2002/3	d+Au	200 GeV	2.74 nb-1
		p+p (L)	200 GeV	0.35 nb-1
Run-4	2003/4	Au+Au	200 GeV	241 μb-1
		Au+Au	62.4 GeV	9 μb-1
Run-5	2005	Cu+Cu	200 GeV	3 nb-1
		Cu+Cu	62.4 GeV	0.19 nb-1
		Cu+Cu	22.4 GeV	2.7 μb-1
		p+p (L)	200 GeV	3.8 pb-1
Run-6	2006	p+p (T+L)	200 GeV	10.7 pb-1
		p+p	62.4 GeV	100 nb-1
Run-7	2007	Au+Au	200 GeV	813 μb-1
Run-8	2007/2008	d+Au	200 GeV	80 nb-1
		p+p (T)	200 GeV	5.2 pb-1
		Au+Au	9.2 GeV	
Run-9	2009	p+p (L)	200 GeV	16 pb-1
		p+p (L)	500 GeV	14 pb-1
Run-10	2010	Au+Au	200 GeV	1.3 nb-1
		Au+Au	62.4 GeV	100 μb-1
		Au+Au	39 GeV	40 μb-1
		Au+Au	7.7 GeV	260 mb-1
Run-11	2011	p+p (L)	500 GeV	27 pb-1
		Au+Au	200 GeV	915 μb-1
		Au+Au	27 GeV	5.2 μb-1
		Au+Au	19.6 GeV	13.7 M events
Run-12	2012	p+p (L)	200 GeV	9.2 pb-1
		p+p (L)	510 GeV	30 pb-1
		U+U	193 GeV	171 μb-1
		Cu+Au	200 GeV	4.96 nb-1
Run-13	2013	p+p (L)	510 GeV	156 pb-1
Run-14	2014	Au+Au	15 GeV	44.2 μb-1
		Au+Au	200 GeV	2.56 nb-1
		He3+Au	200 GeV	134 nb-1

Years	Beam Species and Energies	Science Goals	New Systems Commissioned
2014	15 GeV Au+Au 200 GeV Au+Au	Heavy flavor flow, energy loss, thermalization, etc. Quarkonium studies	Electron lenses 56 MHz SRF STAR HFT, MTD
2015-16	p+p at 200 GeV p+Au, d+Au at 200 GeV	Extract η/s(T) + constrain initial quantum fluctuations More heavy flavor studies	PHENIX MPC-EX Coherent e-cooling test
2017	No Run		Low energy e-cooling upgrade
2018-19	5-20 GeV Au+Au (BES-II)	Search for QCD critical point and onset of deconfinement	STAR iTPC upgrade Partial commissioning of sPHENIX (in 2019)
2020	No Run		Complete sPHENIX installation STAR forward upgrades
2021-22	Long 200 GeV Au+Au with upgraded detectors p+p, p/d+Au at 200 GeV	Jet, di-jet, γ-jet probes of parton transport and energy loss mechanism, color screening for different quarkonia	sPHENIX
2023-24	No Runs		Transition to eRHIC

Figure 3: a)(left) Year, species and proton polarization (**L**ongitudinal or **T**ransverse), $\sqrt{s_{NN}}$, integrated luminosity of RHIC runs. b) (right) Future run schedule and new equipment.

polarized p+p collisions is shown in Fig. 5a; and in Fig. 5b, the plans for future runs are shown.

For this year's run (2014) the full 3 dimensional cooling including electron lenses for partial compensation of the beam-beam tune shift and 56 MhZ storage r.f. for stronger longitudinal focusing were implemented which led to a higher initial luminosity and much longer lifetime of the beam with a more level luminosity load due to the 3d stochatic cooling (Fig. 4). The luminosity performance of RHIC with A+A and polarized p+p collisions is shown in Fig. 5. Notably, the Au+Au $\int \mathcal{L}\, dt$ in 2014 exceeds all previous Au+Au runs combined as did the p+p $\int \mathcal{L}\, dt$ in 2013.

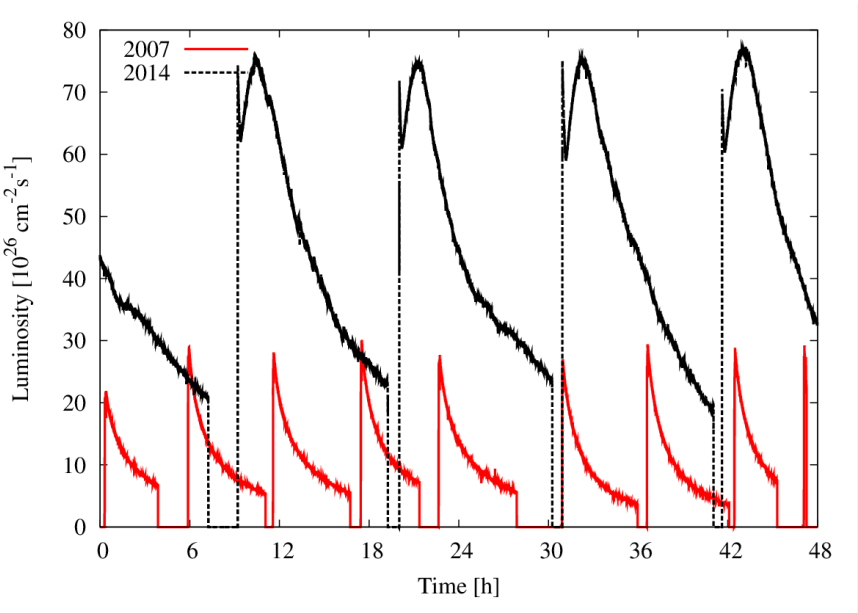

Figure 4: Run-14 luminosity vs. storage time compared to Run-7, courtesy Wolfram Fischer.

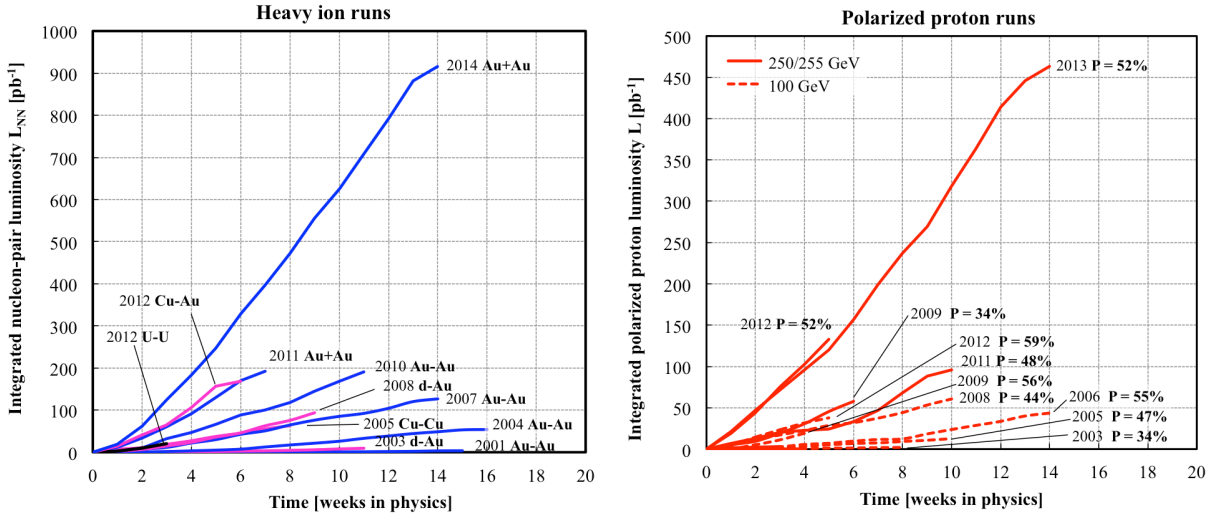

Figure 5: a)(left) Au+Au performance, where the nucleon-pair luminosity is defined as $L_{\rm NN} = A \times B \times L$, where L is the luminosity and A, B are the number of nucleons in the colliding species. b) (right) Polarized p+p performance. Courtesy Wolfram Fischer.

The major future plan for accelerators in Nuclear Physics concerns an electron-ion collider, which if located at BNL will be called eRHIC. A new highly innovative and cost-effective design of eRHIC was proposed this year based on a Fixed Focus Alternating Gradient (FFAG) electron accelerator and an Energy Recovery Linac (Fig. 6).

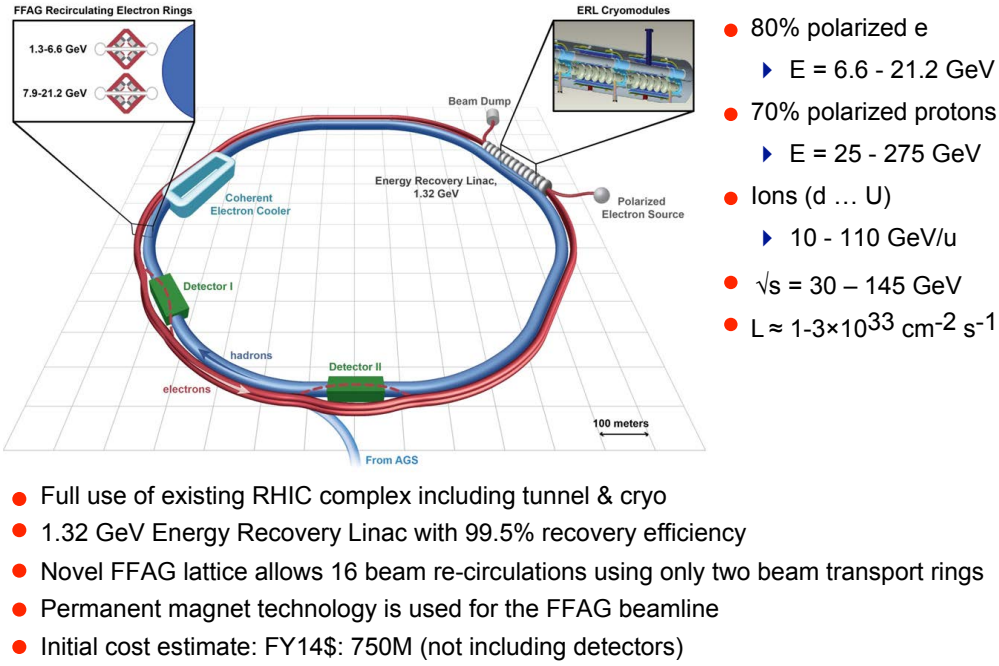

Figure 6: New BNL design for eRHIC with annotations.

4 Detector issues in A+A compared to p+p collisions

A main concern of experimental design in RHI collisions is the huge multiplicity in A+A central collisions compared to p+p collisions. A schematic drawing of a collision of two relativistic Au nuclei is shown in Fig. 7a. In the center of mass system of the nucleus-

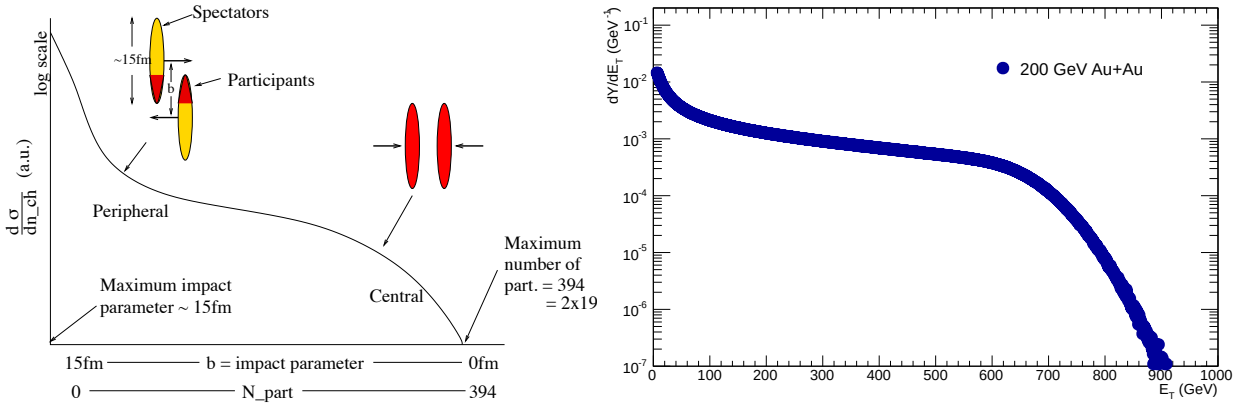

Figure 7: a) (left) Schematic of collision in the N-N c.m. system of two Lorentz contracted nuclei with radius R and impact parameter b. The curve with the ordinate labeled $d\sigma/dn_{\rm ch}$ represents the relative probability of charged particle multiplicity $n_{\rm ch}$ which is directly proportional to the number of participating nucleons, $N_{\rm part}$. b)(right) E_T distribution in Au+Au at $\sqrt{s_{NN}} = 200$ GeV from PHENIX [4].

nucleus collision, the two Lorentz-contracted nuclei of radius R approach each other with impact parameter b. In the region of overlap, the "participating" nucleons interact with each other, while in the non-overlap region, the "spectator" nucleons simply continue on their original trajectories and can be measured in Zero Degree Calorimeters (ZDC), in fixed target experiments, so that the number of spectators can be measured from which the number of participants ($N_{\rm part}$) can be determined for symmetric A+A collisions. The degree of overlap is called the centrality of the collision, with $b \sim 0$, being the most central and $b \sim 2R$, the most peripheral. The maximum time of overlap is $\tau_\circ = 2R/\gamma\, c$ where γ is the Lorentz factor and c is the speed of light in vacuum. The energy of the inelastic collision is predominantly dissipated by multiple particle production, where $N_{\rm ch}$, the number of charged particles produced, or E_T, the energy emitted transverse to the beam direction, is directly proportional [5] to $N_{\rm part}$ as sketched on Fig. 7a. Thus, $N_{\rm ch}$ and E_T in central Au+Au collisions are roughly A times larger than in a p+p collision, as shown in actual events from the STAR and PHENIX detectors at RHIC (Fig. 8).

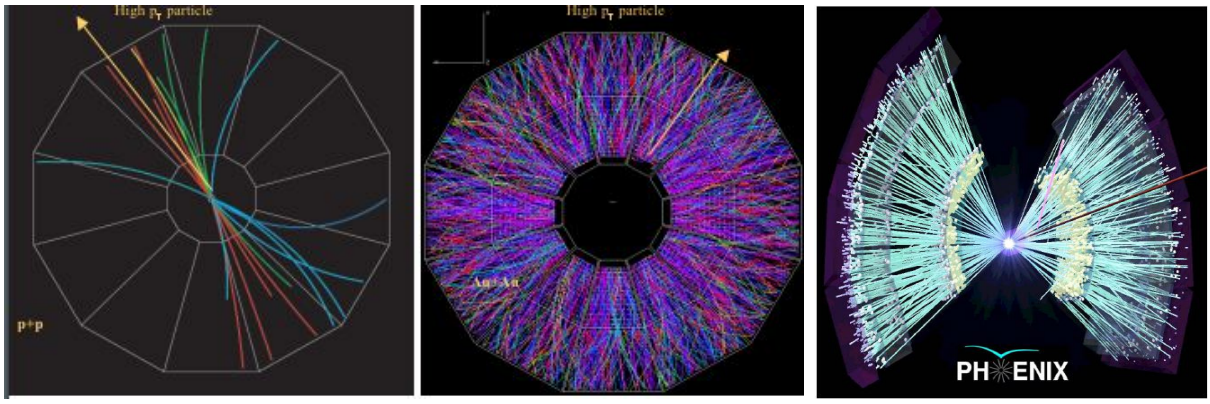

Figure 8: a) (left) A p+p collision in the STAR detector viewed along the collision axis; b) (center) Au+Au central collision at $\sqrt{s_{NN}} = 200$ GeV in STAR; c) (right) Au+Au central collision at $\sqrt{s_{NN}} = 200$ GeV in PHENIX.

At colliders, the impact parameter b can not be measured directly because charged spectators are swept away from zero degrees by the collider magnets. Instead, the centrality of a collision is defined in terms of the upper percentile e.g. top 10%-ile, upper 10−20%-ile, of $N_{\rm ch}$ or E_T distributions as in Fig. 7b. Unfortunately the "upper" and "-ile" are usually not mentioned which sometimes confuses the uninitiated. Also a model is required to derive $N_{\rm part}$ from the measurement so that the derived value of $N_{\rm part}$ at a collider or the number of binary nucleon-nucleon collisions ($N_{\rm coll}$) is model dependent and may have biases.

Since it is a huge task to reconstruct the momenta and identity of all the particles produced in these events, the initial detectors at RHIC [6] concentrated on the measurement of single-particle or multi-particle inclusive variables to analyze RHI collisions, with inspiration from the CERN ISR which emphasized those techniques before the era of jet reconstruction (see, for example, Refs. [7] and [8]). There are at present two major detectors in operation at RHIC, STAR and PHENIX, and there were also two smaller detectors, BRAHMS and PHOBOS, which have completed their program. As may be surmised from Figs. 8a,b and 9a, STAR, which emphasizes hadron physics, is most like a conventional general purpose collider detector, a Time Projection Chamber to detect all charged particles over the full azimuth ($\Delta\phi = 2\pi$) and ± 1 units of pseudo-rapidity (η); while PHENIX (Figs. 8c and 9b),

a) 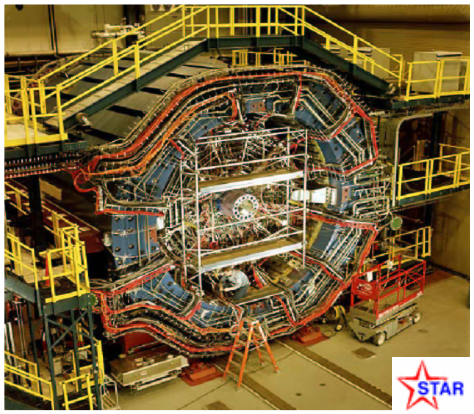 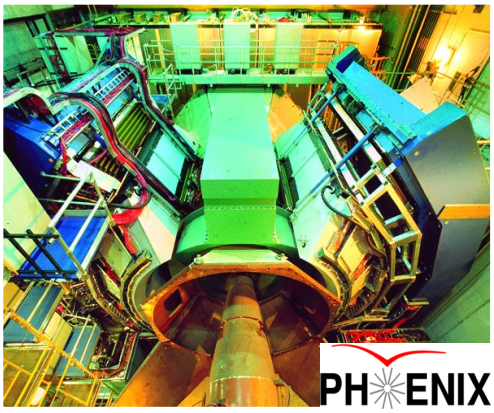 b)

Figure 9: Actual STAR (a) and PHENIX (b) detectors, compare with Figs 8b,c. The direction of the beam is along the axis of the STAR solenoid; and in (b) between the two spectrometer arms (perpendicular to the caption).

is a very high granularity high resolution special purpose detector: a two-arm spectrometer at mid-rapidity, with each arm covering solid angle $|\eta| \leq 0.35, \Delta\phi = 90°$, together with two full-azimuth muon detectors at forward and backward rapidity ($1.1 \leq |\eta| \leq 2.3$).[1] For the present runs, both STAR and PHENIX have excellent particle identification (PID) capability with electromagnetic calorimeters (EMcal) for photon and electron detection and Time of Flight for charged hadrons. PHENIX has a Ring Imaging CHerenkov counter for enhanced electron detection and triggering and small but full azimuth EM calorimeters (MPC) just before each muon arm covering $3.1 \leq |\eta| \leq 3.7$, while STAR obtains enhanced hadron identification using dE/dx in the TPC. For the 2014 run, both PHENIX (VTX, FVTX) and STAR (HFT) are equipped with micro-vertex detectors for tagging Heavy-Flavor c and b quarks via displaced vertices.

The main objectives of buliding RHIC were i) to discover the Quark Gluon Plasma (QGP), which was achieved as I have discussed in detail in review articles based on previous ISSP proceedings [7, 9]; ii) to measure its properties, which were much different than expected, namely a "perfect fluid" of quarks and gluons with their color charges exposed rather than a gas. The latest measurements from RHIC continue to be very interesting.

5 $N_{\rm ch}$, E_T distributions and constituent-quarks as the fundamental elements of particle production

The first experiment specifically designed to measure the dependence of the charged particle multiplicity in high energy p+A collisions as a function of the nuclear size was performed by Wit Busza and collaborators at Fermilab using beams of $\sim 50 - 200$ GeV/c hadrons colliding with various fixed nuclear targets. They found the extraordinary result [10] that the average charged particle multiplicity $\langle N_{\rm ch}\rangle_{hA}$ in hadron+nucleus (h+A) interactions was not simply proportional to the number of collisions (absorption-mean-free-paths), $\langle N_{\rm coll}\rangle = \overline{\nu}$, but increased much more slowly, proportional to the number of participants $\langle N_{\rm part}\rangle$. Thus, relative to h+p collisions (Fig. 10a) [11]:

$$R_A = \langle N_{\rm ch}\rangle_{hA} \,/\, \langle N_{\rm ch}\rangle_{hp} = \langle N_{\rm part}\rangle_{hA} \,/\, \langle N_{\rm part}\rangle_{hp} = (1+\overline{\nu})/2 \qquad . \tag{1}$$

[1] The detector is so non-conventional that it made the cover of Physics Today, October 2003.

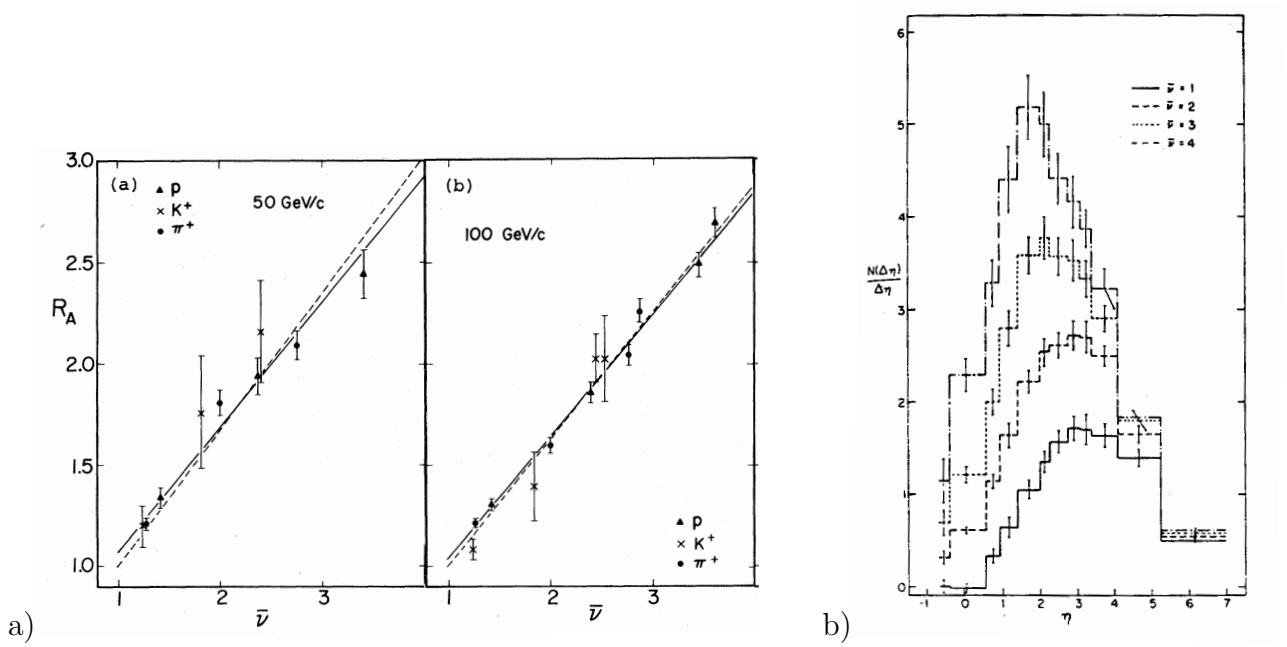

Figure 10: a) $R_A = \langle N_{\rm ch}\rangle_{hA} / \langle N_{\rm ch}\rangle_{hp}$ as a function of the average thickness of each nucleus given in terms of the mean free path, $\overline{\nu} = \langle N_{\rm coll}\rangle$ [11] for 50 and 100 GeV/c h+A collisions; b) Charged particle multiplicity density, $dN_{\rm ch}/d\eta$, as a function of A (represented by $\overline{\nu}$) for 200 GeV/c p+A collisions [12].

Since the different projectiles, $h = \pi^+, K^+, p$ in Fig. 10a have different mean free paths, the fit to the same straight line in terms of $\overline{\nu}$ is convincing.

The other striking observation (Fig. 10b) [12] was that a relativistic incident proton could pass through e.g. $\nu = 4$ absorption-mean-free-paths of a target nucleus and emerge from the other side; and furthermore there was no intra-nuclear cascade of produced particles (a stark difference from what would happen to the same proton in a macroscopic 4 mean-free-path hadron calorimeter). In the forward fragmentation region of 200 GeV/c p+A collisions, within 1 unit of rapidity from the beam, $y^{\rm beam} = 6.06$, there was essentially no change in $dN_{\rm ch}/d\eta$ as a function of A, while at mid-rapidity ($\eta \approx y^{\rm cm}_{NN} = 3.03$), $dN_{\rm ch}/d\eta$ increased with A together with a small backward shift of the peak of the distribution resulting in a huge relative increase of multiplicity in the target fragmentation region, $\eta < 1$ in the laboratory system. These striking features of the ~ 200 GeV/c fixed target hadron-nucleus data ($\sqrt{s_{NN}} \sim 19.4$ GeV) showed the importance of taking into account the time and distance scales of the soft multi-particle production process including quantum mechanical effects.

5.1 The Wounded Nucleon Model

The observations in Fig. 10 had clearly shown that the target nucleus was rather transparent so that a relativistic incident nucleon could make many successive collisions while passing through the nucleus, and emerge intact. Immediately after a relativistic nucleon interacts inside a nucleus, the only thing that can happen consistent with relativity and quantum mechanics is for it to become an excited nucleon with roughly the same energy and reduced longitudinal momentum and rapidity. It remains in that state inside the nucleus because the uncertainty principle and time dilation prevent it from fragmenting into particles until it is well outside the nucleus. This feature immediately eliminates the possibility of a cascade

in the nucleus from the rescattering of the secondary products. If one makes the further assumptions that an excited nucleon interacts with the same cross section as an unexcited nucleon and that the successive collisions of the excited nucleon do not affect the excited state or its eventual fragmentation products [13], this leads to the conclusion (c. 1977) that the elementary process for particle production in nuclear collisions is the excited nucleon, and to the prediction that the multiplicity in nuclear interactions should be proportional to the total number of projectile and target participants, rather than to the total number of collisions, or $R_A = \langle N_{\rm ch}\rangle_{hA} \,/\, \langle N_{\rm ch}\rangle_{hp} = \langle N_{\rm part}\rangle_{hA} \,/\, \langle N_{\rm part}\rangle_{hp} = (1+\overline{\nu})/2$, as observed. This is called the Wounded Nucleon Model (WNM) [14] and, in the common usage, Wounded Nucleons (WN) are called participants. In a later model from the early 1980's, the Additive Quark Model, AQM [15], constituent-quark participants were introduced; but the AQM is actually a model of particle production by color-strings in which only one color-string can be attached to a constituent-quark participant, effectively a projectile quark participant model.

5.2 Extreme Independent Models

The models mentioned above are examples of Extreme Independent Models in which the effect of the nuclear geometry of the interaction can be calculated independently of the dynamics of particle production which can be taken directly from experimental measurements. The nuclear geometry is represented by the relative probability, w_n per A+B interaction for a given number n of fundamental elements, in the present case, number of collisions ($N_{\rm coll}$), number of nucleon participants (wounded nucleon model-WNM [14]), number of constituent-quark participants (N_{qp}), number of color strings (AQM). The dynamics of particle production, the $N_{\rm ch}$ or E_T distribution of the fundamental element, is taken from the measured p+p data in the same detector: e.g. the measured $N_{\rm ch}$ distribution for a p+p collision represents: 1 collision; 2 participants (WNM); a predictable convolution of constituent-quark-participants (NQP), or projectile-quark-participants (AQM). Glauber calculations of the nuclear geometry (w_n) together with the p+p measurement provide a prediction for the A+B measurement in the same detector as the result of particle production by multiple independent fundamental elements.

I became acquainted with these models in my first talk at a Quark Matter conference (QM1984) where I presented measurements of transverse energy distributions from p+p and α+α interactions at $\sqrt{s_{_{NN}}}$ =31 GeV at the CERN-ISR (Fig. 11a [18, 19]). The transverse energy, E_T, is a multiparticle variable defined as the sum

$$\mathrm{E}_T = \sum_i E_i \, \sin\theta_i \qquad d\mathrm{E}_T(\eta)/d\eta = \sin\theta(\eta)\, dE(\eta)/d\eta, \tag{2}$$

where θ is the polar angle, $\eta = -\ln\tan\theta/2$ is the pseudorapidity, E_i is by convention taken as the kinetic energy for baryons, the kinetic energy + 2 m_N for antibaryons, and the total energy for all other particles, and the sum is taken over all particles emitted into a fixed solid angle for each event.

The transverse energy was introduced by high energy physicists [16, 17] as an improved method to detect and study the jets from hard-scattering compared to high p_T single particle spectra by which hard-scattering was discovered in p+p collisions and used as a hard-probe in Au+Au collisions at RHIC. However, it didn't work as expected: E_T distributions, like $N_{\rm ch}$ distributions, are dominated by soft particles near $\langle p_T\rangle$ (e.g. see Ref. [8] for details).

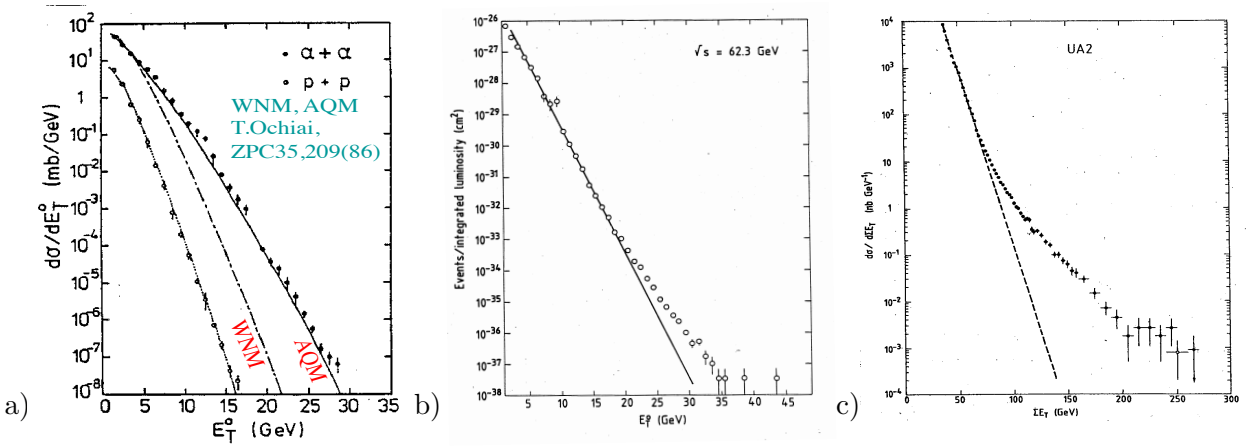

Figure 11: (a) E_T distributions in p+p, α+α [18] at $\sqrt{s_{NN}}$ =31 GeV, with AQM and WNM calculations [21]. (b),(c) E_T distributions with breaks indicating jets: (b) p+p $\sqrt{s}$ =62.3 GeV [22]; (c) $d\sigma/dE_T$ (nb/GeV) vs. E_T for $\bar{p}$+p $\sqrt{s}$ =540 GeV [23].

Nevertheless, it was claimed at the conference [20], in comments to my talk, that the deviation from the WNM in Fig. 11a was due to jets, but in both proceedings [19, 20] it was demonstrated that [20] "there is no ... sign of jets. This indicates that soft processes are still dominant, and that we are still legimately testing the WNM at these high values of E_T." As shown in Fig. 11a, the the AQM [21], rather than the WNM, followed the data. Jets do appear in E_T distributions as a break $\lesssim 10^{-5}$ down in cross section (Figs. 11b,c).

5.3 E_T and $N_{\rm ch}$ distributions cut on centrality

At RHIC, following the style of the CERN SpS rather than the BNL-AGS fixed target heavy ion program, E_T and $N_{\rm ch}$ distributions were not generally shown. The measurements were presented cut in centrality in the form $\langle dN_{\rm ch}{}^{\rm AA}/d\eta\rangle\,/(\langle N_{\rm part}\rangle\,/2)$ vs. $\langle N_{\rm part}\rangle$ (Fig. 12), which would be a constant equal to $\langle dN_{\rm ch}{}^{\rm pp}/d\eta\rangle$ if the WNM worked. The measurements

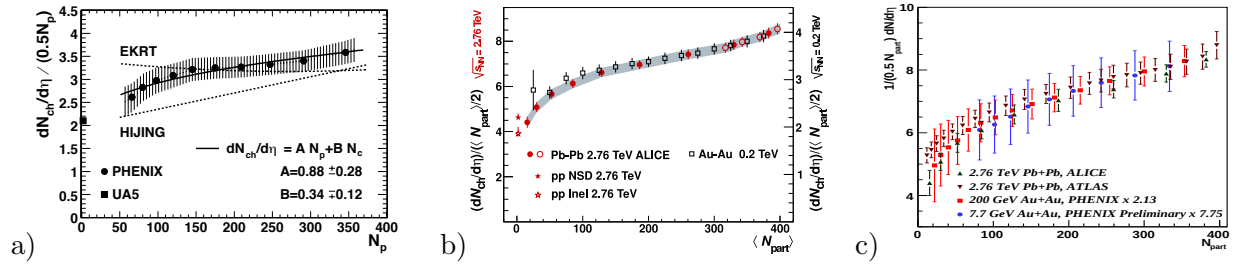

Figure 12: (a) PHENIX, Au+Au, $\sqrt{s_{NN}}$ =130 GeV [24]; (b) ALICE, Pb+Pb, $\sqrt{s_{NN}}$ =2.76 TeV [26]; (c) PHENIX preliminary Au+Au, $\sqrt{s_{NN}}$ =7.7 GeV compared to the data at larger $\sqrt{s_{NN}}$ [27].

clearly deviate from the WNM (Fig. 12a) [24]; so the PHENIX collaboration, inspired by the preceding article in the journal [25], fit their data to the two-component model:

$$dN_{\rm ch}{}^{AA}/d\eta = (dN_{\rm ch}{}^{pp}/d\eta)\;[(1-x)\;\langle N_{\rm part}\rangle\,/2 + x\;\langle N_{\rm coll}\rangle] \qquad (3)$$

where the $N_{\rm coll}$ term implied a hard-scattering component for E_T and $N_{\rm ch}$, known to be absent in p+p collisions [2] (recall Fig. 11). A decade later, the first measurement from Pb+Pb

[2]It was noted in Ref. [24] that hard-scattering was not a unique interpretation. The shape of the centrality dependences of $dE_T{}^{AA}/d\eta$ parameterized as $N_{\rm part}{}^{\alpha}$ were the same for Pb+Pb at $\sqrt{s_{NN}}$ =17.6 GeV at the

collisions with $\sqrt{s_{NN}}$ =2.76 TeV at the LHC Fig. 12b [26], showed exactly the same shape vs. $N_{\rm part}$ as the RHIC Au+Au data at $\sqrt{s_{NN}}$ =200 GeV, although $\langle N_{\rm coll}\rangle$ is a factor of 1.6 larger and the hard-scattering cross section is more than a factor of 20 larger. This strongly argued against a hard-scattering component and for a nuclear geometrical effect, which was reinforced by a PHENIX preliminary measurement in Au+Au at $\sqrt{s_{NN}}$ =7.7 GeV (Fig. 12c) [27] which also showed the same shape for the evolution of $\left\langle dN_{\rm ch}{}^{\rm AA}/d\eta\right\rangle/(\langle N_{\rm part}\rangle/2)$ with $N_{\rm part}$ as the $\sqrt{s_{NN}}$ =200 and 2760 GeV measurements. It had previously been proposed that the number of constituent-quark participants provided the nuclear geometry that could explain the RHIC Au+Au data without the need to introduce a hard-scattering component [28]. However an asymmetric system is necessary in order to distinguish the NQP model from the AQM so the two models were applied to the RHIC d+Au data.

5.4 The number of constituent-quark participants model (NQP)

The massive constituent-quarks [29], which form mesons and nucleons (e.g. a proton=uud), are relevant for static properties and soft physics with $p_T\lesssim$1.4 GeV/c. They are complex objects or quasiparticles [30] made of the massless partons (valence quarks, gluons and sea quarks) of DIS [31] such that the valence quarks acquire masses $\approx 1/3$ the nucleon mass with radii $\approx$ 0.3 fm when bound in the nucleon. With smaller resolution one can see inside the bag to resolve the massless partons which can scatter at large angles according to QCD. At RHIC, hard-scattering starts to be visible as a power law above soft (exponential) particle production only for $p_T > 1.4$ GeV/c at mid-rapidity (Fig 13a), where $Q^2 = 2p_T^2 = 4$ (GeV/c)^2 which corresponds to a distance scale (resolution) < 0.1 fm.[3]

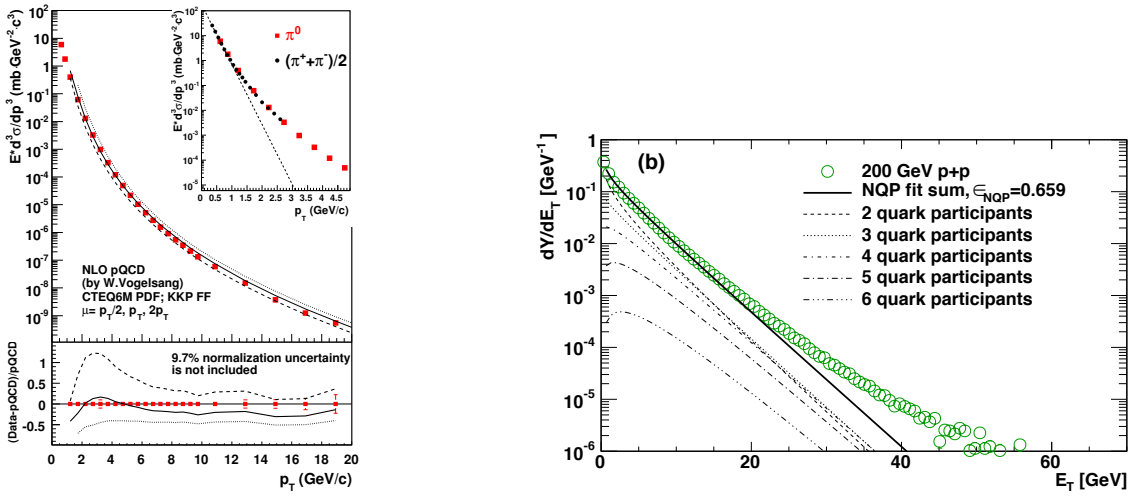

a)

Figure 13: (a) Invariant cross section of π^0 vs. p_T at mid-rapidity in p+p collisions at $\sqrt{s}$ =200 GeV [34]. The inset shows the transition from an exponental to a power-law in the range $1 < p_T < 2$ GeV/c (b) PHENIX deconvolution of p+p E_T distribution at $\sqrt{s}$ =200 GeV [4]

CERN SpS and Au+Au at $\sqrt{s_{NN}}$ =130 GeV, with $\alpha = 1.1$ and $\alpha = 1.16 \pm 0.04$, respectively. The LHC data 10 years later [26] gave $\alpha = 1.19 \pm 0.02$ for Pb+Pb at $\sqrt{s_{NN}}$ =2760 GeV, again the same shape.

[3]Shuryak and collaborators recently made similar arguments about resolution in separating hard from soft processes although their mechanism for soft particle and QGP production was 2 color strings per wounded nucleon from Pomeron exchange [32].

A standard Monte Carlo Glauber calculation is used to assemble the initial positions of all the nucleons. Then three quarks are distributed around the center of each nucleon according to the proton charge distribution $\rho(\vec{r}) \propto e^{-\sqrt{12}\, r/r_{\rm rms}}$, where $r_{\rm rms} = 0.81$ fm is the rms charge radius of the proton [33]. The q–q inelastic scattering cross section is adjusted to 9.36 mb at $\sqrt{s}$ =200 GeV to give the correct p+p inelastic cross section (42 mb) and then used in the A+B calculations.

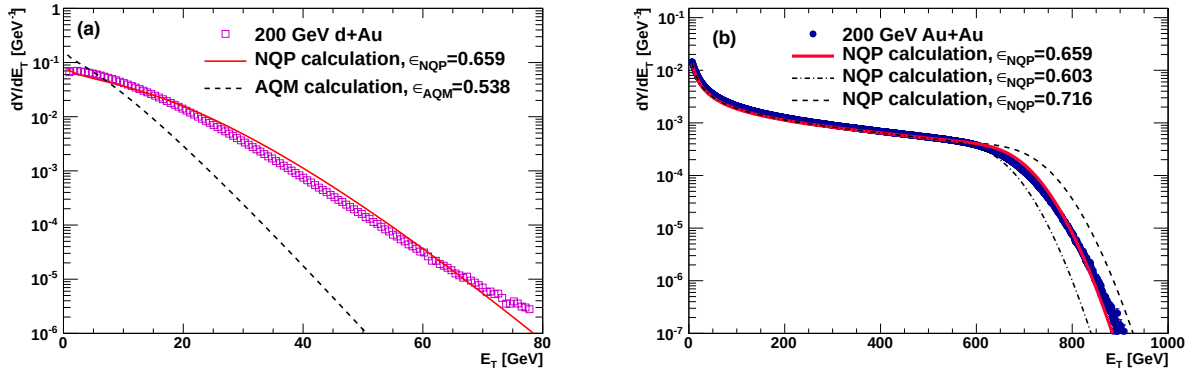

Figure 14: PHENIX NQP calculations [4] based on the E_T distribution of a constituent-quark participant from Fig. 13b for: (a) d+Au (also AQM), (b) Au+Au E_T distributions at $\sqrt{s_{NN}}$ =200 GeV.

Fig. 13b shows the deconvolution of the p+p E_T distribution to the sum of 2–6 constituent-quark participants from which the E_T distribution of a constituent-quark is determined and applied to d+Au (Fig. 14a) and Au+Au (Fig. 14b) reactions in the same detector.

The NQP calculations closely follow the measured d+Au and Au+Au E_T distributions in shape and magnitude over a range of more than 1000 in cross section. A complete calculation was also done for the AQM which fails to describe the d+Au data (Fig. 14a). The conclusion is that the number of constituent-quark participants determines the $N_{\rm ch}$ and E_T distributions and that the AQM calculation which describes the α–α data at $\sqrt{s_{NN}}$ =31 GeV (Fig. 11a) is equivalent to the NQP in the symmetric system.

The NQP model was also applied to the centrality-cut PHENIX data by making a plot of $dE_T/d\eta$ for a given centrality bin as a function of the number of constituent-quark participants N_{qp} in the bin for Au+Au collisions at $\sqrt{s_{NN}}$ = 62.4, 130 and 200 GeV (Fig. 15a).

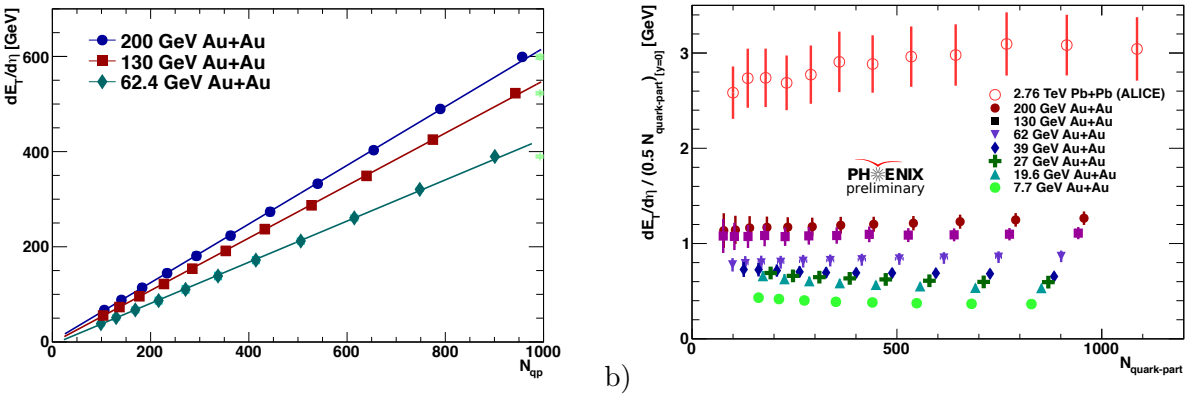

a) b)

Figure 15: PHENIX [4]: (a) $dE_T/d\eta$ vs. N_{qp} ; (b) $dE_T/d\eta/(N_{qp}/2)$ vs. N_{qp}

The data for each $\sqrt{s_{NN}}$ are well described by a straight line and all are consistent with a zero intercept. This means that $d\mathrm{E}_T/d\eta$ is strictly proportional to N_{qp} (Fig 15a) so that $d\mathrm{E}_T/d\eta/(N_{qp}/2)$ vs. N_{qp} is a constant for $\sqrt{s_{NN}} > 39$ GeV (Fig 15b) even up to the LHC $\sqrt{s_{NN}} = 2.76$ TeV. This brought up a very interesting question, with a very important and fundamental answer.

Most experiments at RHIC, starting with PHENIX (Fig. 12) [24] had successfully fit their measurements of $d\mathrm{E}_T/d\eta$ or $dN_{\mathrm{ch}}/d\eta$ as a function of centrality (represented by N_{part}) to the two-component model (Eq. 3). Also, both the ATLAS [35] and ALICE [36] experiments at the LHC computed the ansatz, $[(1-x)\langle N_{\mathrm{part}}\rangle/2 + x\ \langle N_{\mathrm{coll}}\rangle]$, in event-by-event Glauber Monte Carlo calculations which fit their forward E_T measurements used to define centrality in Pb+Pb collisions. ALICE realized that the combination of the two components N_{part} and N_{coll} in the ansatz represented the number of emitting sources of particles, which they named "ancestors". Since the number of constituent-quarks N_{qp} also represents the number of emitting sources in a simple linear relationship, Bill Zajc of PHENIX suggested that "the success of the two component model is not because there are some contributions proportional to N_{part} and some going as N_{coll}, but because a particular linear combination of N_{part} and N_{coll} turns out to be an empirical proxy for the number of contsituent-quarks." We had a nice table of $\langle N_{\mathrm{part}}\rangle$, $\langle N_{qp}\rangle$, $\langle N_{\mathrm{coll}}\rangle$ as a function of centrality in Au+Au collisions at $\sqrt{s_{NN}}$ =200 GeV, so it did not take very long for me to verify the striking result that indeed it was true: with $x = 0.08$, the ratio $\langle N_{qp}\rangle/[(1-x)\langle N_{\mathrm{part}}\rangle/2 + x\ \langle N_{\mathrm{coll}}\rangle] = 3.88$ on the average and varies by less than 1% over the entire centrality range in 5% bins except for the most peripheral bin where it is 5% low (Table 1). This result clearly demonstrates that the ansatz works because the particular linear combination of N_{part} and N_{coll} turns out to be an empirical proxy for N_{qp} and not because the N_{coll} term implies hard-scattering.

Centrality	$\langle N_{part}\rangle$	$\langle N_{qp}\rangle$	$\langle N_{\mathrm{coll}}\rangle$	ansatz	$\langle N_{\mathrm{qp}}\rangle$/ansatz
0-5%	350.9 ± 4.7	956.6 ± 16.2	1064.1 ± 110.0	246.5	3.88
5-10%	297.0 ± 6.6	789.8 ± 15.3	838.0 ± 87.2	203.7	3.88
10-15%	251.0 ± 7.3	654.2 ± 14.5	661.1 ± 68.5	168.3	3.89
15-20%	211.0 ± 7.3	540.2 ± 12.3	519.1 ± 53.7	138.6	3.90
20-25%	176.3 ± 7.0	443.3 ± 10.4	402.6 ± 39.5	113.3	3.91
25-30%	146.8 ± 7.1	362.8 ± 12.2	311.9 ± 31.8	92.5	3.92
30-35%	120.9 ± 7.0	293.3 ± 11.0	237.8 ± 24.2	74.6	3.93
35-40%	98.3 ± 6.8	233.5 ± 9.2	177.3 ± 18.3	59.4	3.93
40-45%	78.7 ± 6.1	182.7 ± 6.8	129.6 ± 12.6	46.6	3.92
45-50%	61.9 ± 5.2	140.5 ± 5.3	92.7 ± 9.0	35.9	3.91
50-55%	47.6 ± 4.9	105.7 ± 5.5	64.4 ± 8.1	27.0	3.91
55-60%	35.6 ± 5.1	77.3 ± 6.8	43.7 ± 7.6	19.9	3.89
60-65%	26.1 ± 4.7	55.5 ± 7.1	29.0 ± 6.5	14.3	3.87
65-70%	18.7 ± 4.0	39.0 ± 6.7	18.8 ± 5.3	10.1	3.86
70-75%	13.1 ± 3.2	27.0 ± 4.9	12.0 ± 3.6	7.0	3.86
75-80%	9.4 ± 2.1	19.0 ± 3.2	7.9 ± 2.2	5.0	3.83
80-92%	5.4 ± 1.2	10.3 ± 1.5	4.0 ± 1.0	2.8	3.67
p+p	2	2.99 ± 0.05	1	1	2.99

Table 1: Verification that the ansatz, $[(1-x)\langle N_{\mathrm{part}}\rangle/2 + x\ \langle N_{\mathrm{coll}}\rangle]$, from Eq. 3, with $x = 0.08$, is a proxy for N_{qp}. The errors quoted on $\langle N_{\mathrm{part}}\rangle$, $\langle N_{qp}\rangle$, $\langle N_{\mathrm{coll}}\rangle$ are correlated and largely cancel in the $\langle N_{qp}\rangle$/ansatz ratio. For $x = 0.09$ the average $\langle N_{qp}\rangle$/ansatz=3.81, the maximum variation is less than 1.6%, but 4% low in the most peripheral bin.

The fact that the $\langle N_{qp}\rangle$/ansatz ratio drops from an average of 3.88 for Au+Au collisions to 2.99 for p+p collisions is also interesting. This is consistent with the PHOBOS [37] result that a fit of Eq. 3 to $\langle dN_{\rm ch}{}^{AA}/d\eta\rangle$ with $x = 0.09$ leaving $\langle dN_{\rm ch}{}^{pp}/d\eta\rangle$ as a free parameter gives the result $\langle dN_{\rm ch}{}^{pp}/d\eta\rangle = 2.70$ which is above the measured inelastic value of 2.29. The lower value of $\langle N_{qp}\rangle$/ansatz for p+p would then give a value of $2.70 \times 2.99/3.88 = 2.08$ (2.12 for $x = 0.09$) for $\langle dN_{\rm ch}{}^{pp}/d\eta\rangle$, much closer to the measured value. In that same paper, PHOBOS also noted that their data were consistent with a constant value of x from $\sqrt{s_{NN}}$ =19.6 to 200 GeV (more recently extended to $\sqrt{s_{NN}}$ =2.76 TeV [38]) which indicated that the fraction of hard-processes contributing to multiplicity did not increase over a huge range of $\sqrt{s}$ even though the hard-scattering cross section greatly increased over this same range.

5.5 Constituent-quark participants resolve several outstanding puzzles

PHOBOS also made some very nice measurements of the charged particle multiplicity over the full rapidity range, not just mid-rapidity. The total charged multiplicity $N_{\rm ch}|_{|\eta|<5.4}$ was measured and $N_{\rm ch}|_{|\eta|<5.4}/\langle N_{\rm part}/2\rangle$ plotted as a function of centrality for $\sqrt{s_{NN}}$ =19.6, 62.4,130, and 200 GeV (Fig. 16a) [39]. At first glance the data appear to follow the WNM because the multiplicity/per nucleon pair $N_{\rm ch}|_{|\eta|<5.4}/\langle N_{\rm part}/2\rangle$ appears to be constant in Au+Au collisions. However, the true believers, e.g. Ref. [40], claim that the WNM does not work because the value in Au+Au collisions is much larger than the p+p value shown; but "still the proportionality of these multiplicities to the number of participants holds" [40].

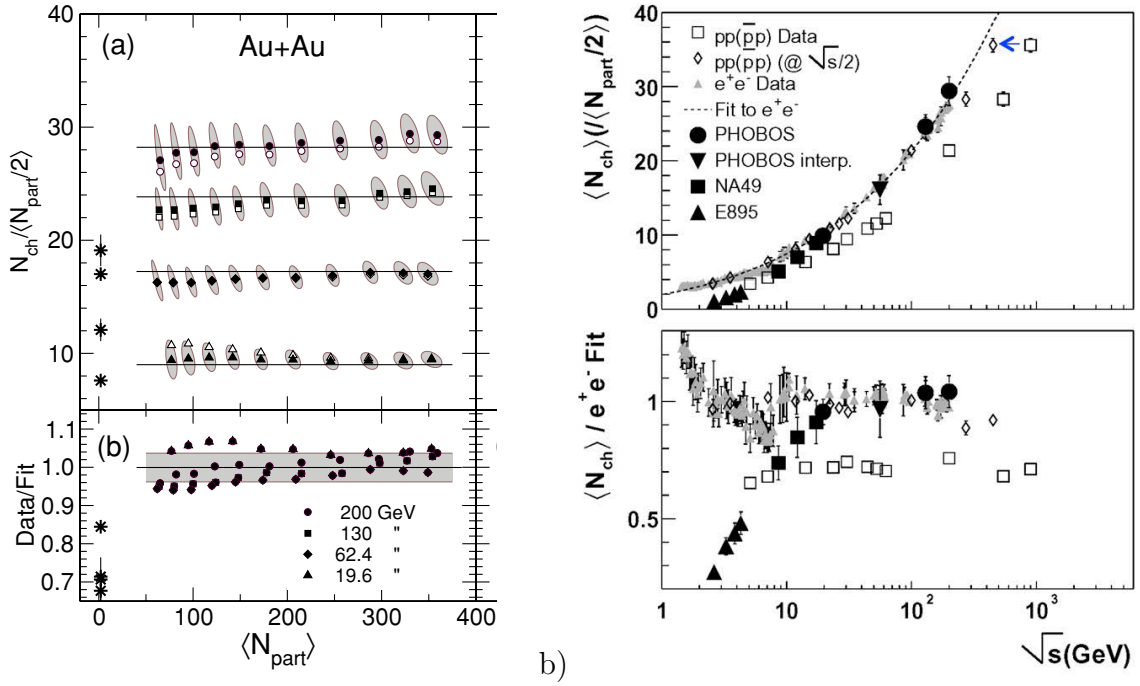

b)

Figure 16: a) Total charged multiplicity per nucleon pair $N_{\rm ch}/\langle N_{\rm part}/2\rangle$ vs. centrality, $N_{\rm part}$, for the $\sqrt{s_{NN}}$ indicated. Open points are the measured $N_{\rm ch}|_{|\eta|<5.4}/(\langle N_{\rm part}/2\rangle$; solid points are extrapolated to $|\eta| \leq y_{\rm beam}$. b) Total charged multiplicity per nucleon pair in p+p and A+A collisions as a function of c.m. energy $\sqrt{s}$ compared to $e^+ + e^-$ collisions [41].

In fact, the difference between the p+p and Au+Au values may be related to another interesting observation by PHOBOS [41] that the "leading particle effect" in p+p collisions, as discovered by Zichichi and collaborators [42]—in which the total multiplicity at c.m. energy $\sqrt{s_{\rm pp}}$ is equal to that in e^+e^- collisions at $\sqrt{s_{\rm ee}} = \sqrt{s_{\rm pp}}/2$ (the "effective energy") (Fig. 16b) because the leading protons carry away half the p+p c.m. energy—is absent in A+A collisions where the leading protons can reinteract. This observation seems to contradict the WNM, in which the key assumption is that what counts is whether or not a nucleon was struck, not how many times it was struck.

Both these effects can be reconciled by constituent-quark participants.

In the NQP model (Table 1), the $\langle N_{qp}/N_{\rm part}\rangle$ is 1.5 for a p+p collision but rises to 2.27–2.73 (a factor of 1.51–1.82) for the more central (0-50%, $\langle N_{\rm part}\rangle > 60$) Au+Au collisions plotted in Fig. 16a. This would correspond to an increase in $N_{\rm ch}/\langle N_{\rm part}/2\rangle$ by a factor of ~ 1.5 as observed. It also might explain the slight rise of the open points with increasing $N_{\rm part}$. Similarly, the increase in "effective energy" for particle production shown by the increase in $N_{\rm ch}/\langle N_{\rm part}/2\rangle$ from p+p to Au+Au collisions is due to an increase in the number of (constituent-quark) participants, not because of additional collisions of a given nucleon-participant. Furthermore, the factor 1.5 decrease in $N_{\rm ch}/\langle N_{\rm part}/2\rangle$ from Au+Au to p+p corresponds to a reduction in $\sqrt{s}$ for the observed $N_{\rm ch}/\langle N_{\rm part}/2\rangle$ from 200 to 100 GeV p+p collisions on Fig. 16b, the same factor of 2 discussed in the original measurement [41]. Thus, the NQP model rather than the WNM preserves the assumption in these "extreme-independent" participant models that successive collisions of a participant do not increase its particle emission while explaining these two interesting observations.

Another argument against the $N_{\rm part}$, $N_{\rm coll}$ ansatz representing actual hard-collisions rather than simply being a proxy for constituent-quark participants concerns the measurement of elliptic flow in central U+U collisions [43].

6 Collective Flow

For many years, since the days of the Bevalac [44], collective flow [45] has been observed in A+A collisions over the full range of energies studied, from incident kinetic energy of $100A$ MeV to c.m. energy of $\sqrt{s_{NN}} = 2.76$ TeV, and thought to be a distinguishing feature of A+A collisions compared to either p+p or p+A collisions. Collective flow, or simply flow, is a collective effect which can not be obtained from a superposition of independent N+N collisions. I first present a short review (details can be found in previous ISSP proceedings [7, 9]) and then move on to the newer results.

Immediately after an A+A collision, the overlap region defined by the nuclear geometry is almond shaped (see Fig 17a) with the shortest axis along the impact parameter vector. The different pressure gradients along the short and long axes of the ellipse break the ϕ symmetry of the problem and create an azimuthal angular dependence of the semi-inclusive single particle spectrum with respect to the reaction plane, $\phi - \Phi_R$, which is represented by an expansion in harmonics [48], where the angle of the reaction plane Φ_R is defined to be along the impact parameter vector, the x axis in Fig. 17a:

$$\frac{Ed^3N}{dp^3} = \frac{d^3N}{p_T dp_T dy d\phi} = \frac{d^3N}{2\pi\, p_T dp_T dy}\left[1 + \sum_n 2v_n \cos n(\phi - \Phi_R)\right]. \qquad (4)$$

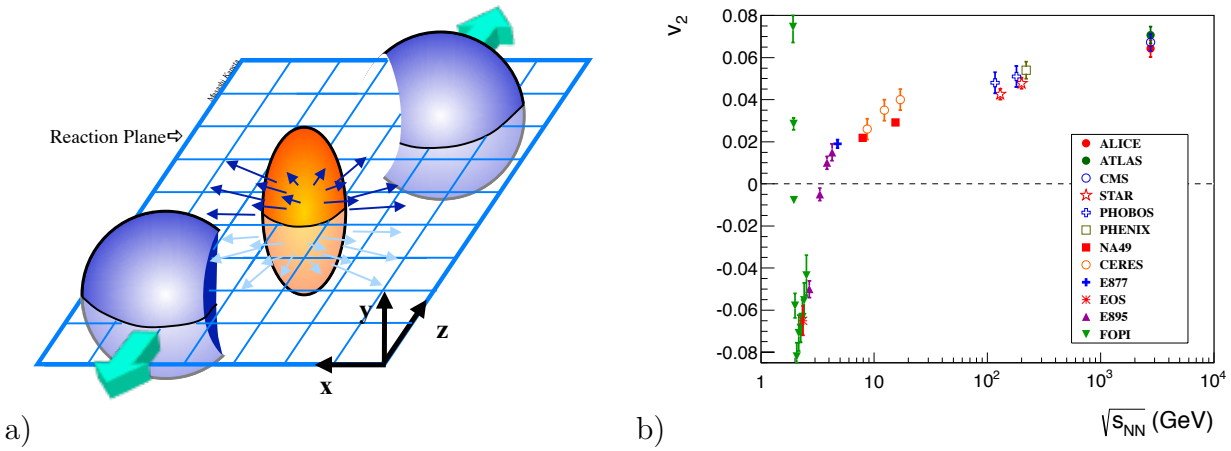

Figure 17: (a) Almond shaped overlap zone generated just after an A+A collision where the incident nuclei are moving along the $\pm z$ axis. The reaction plane by definition contains the impact parameter vector (along the x axis) [46]. (b) v_2 for charged particles integrated over p_T at $\sqrt{s_{NN}}$ =2.76 TeV for 20–30% centrality compared to the measurements at lower $\sqrt{s_{NN}}$ at the same centrality [47].

The Fourier coefficient v_2, called elliptic flow, is predominant at mid-rapidity. The evolution of v_2 with $\sqrt{s_{NN}}$ (Fig. 17b) [47] is the result of competing processes. At very low $\sqrt{s_{NN}}$ corresponding to values of $\sim 100A$ MeV [49] the main effect among many others is from nuclei bouncing off each other and breaking to fragments, which is sensitive to the equation of state of the nuclei—soft, like sponges, hard like billiard balls? The negative v_2 at larger $\sqrt{s_{NN}}$ is produced by the effective "squeeze-out" (in the y direction) of the produced particles by slow moving minimally Lorentz-contracted spectators (as in Fig. 17a) which block the particles emitted in the reaction plane. With increasing $\sqrt{s_{NN}}$, the spectators move faster and become more contracted so the blocking stops. The increase of v_2 with $\sqrt{s_{NN}}$ is generally described by hydrodynamics in the QGP region, but is also described by hadron transport theories for $\sqrt{s_{NN}} \lesssim 10$ GeV [50].

Flow measurements contributed two of the most important results about the properties of the QGP: i) the scaling of v_2 of identified particles at mid-rapidity with the number of constituent-quarks n_q in the particle—v_2/n_q scales with the transverse kinetic energy per constituent-quark, KE_T/n_q, because particles have not formed at the time flow develops; ii) the persistence of flow for $p_T > 1$ GeV/c which implied that the viscosity is small [51], perhaps as small as a quantum viscosity bound from string theory [52], $\eta/s = 1/(4\pi)$ where η is the shear viscosity and s the entropy density per unit volume. This led to the description of the "sQGP" produced at RHIC as "the perfect fluid".

New insight came in 2013, when measurements in p+Pb at LHC and d+Au at RHIC observed what looked very much like collective flow in these systems that were believed to be too small to support collective effects. This was the reason for the He^3+Au run at RHIC in 2014, to see whether triangular flow, v_3, would be more prominent with a 3 nucleon projectile. The improvement of the p+Au and d+Au measurements this year to identified pions and protons strengthened the case that the observed v_2 in these small systems is really hydrodynamic collective flow.

Figure 18a [53] shows the two-particle correlation function in d+Au (Eq. 5) fit with terms from c_1 to c_4 where the solid line is the fit and only the c_1 (dashes) and c_2 (dots) make significant contribution.

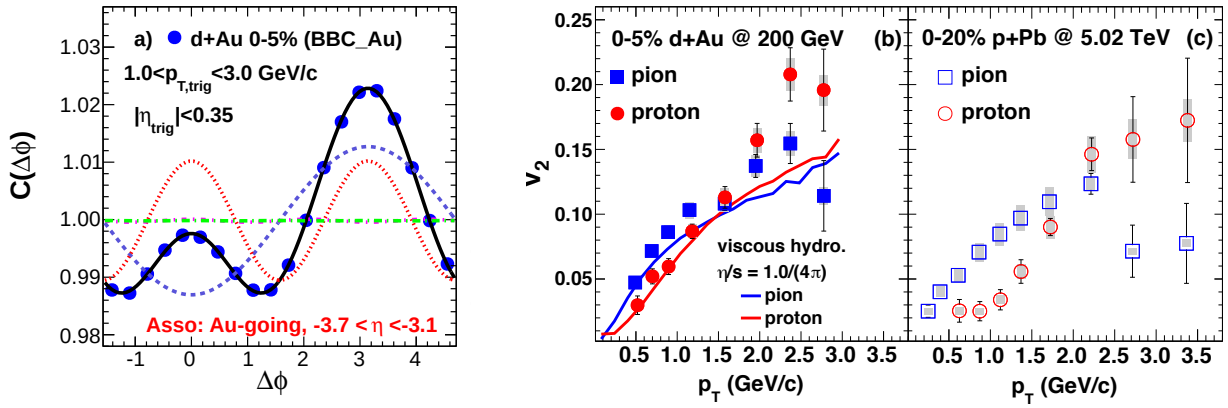

Figure 18: (a) PHENIX [53] two-particle azimuthal correlation function (Eq. 5) for $1.0 < p_{\rm T,trig} < 3.0$ GeV/c, $|\eta_{\rm trig}| < 0.35$, in central (0-5%) d+Au collisions at RHIC. $v_2(p_T)$ for identified $\pi^{\pm}$ $p^{\pm}$ by the standard reaction plane method (Eq. 4) for (b) central d+Au collisions at RHIC ($\sqrt{s_{_{NN}}}$ =200 GeV) and (c) central p+Pb collisions at LHC ($\sqrt{s_{_{NN}}}$ =5.02 TeV).

$$\frac{dN_{ta}}{d\phi_t d\phi_a} = C(\phi_t - \phi_a) \propto \left[1 + \sum_n 2\, c_n \cos n(\phi_t - \phi_a)\right], \qquad c_n \equiv (v_n)_t (v_n)_a \tag{5}$$

The c_1 comes into play because the trigger particle t is a charged track at mid-rapidity while the associated particle a is a count in an MPC tower ($\delta\eta \times \delta\phi \approx 0.12 \times 0.18$) from π^0 or η meson decay photons at $-3.7 \leq \eta_{\rm tower} \leq -3.1$. Also, there is no evidence of a di-jet contribution because the large pseudorapidity gap between t and a is beyond that of a di-jet. Thus, the long-range correlation in Fig. 18a which is not seen in p+p comparison data but has the same properties as collective flow in Au+Au collisions is consistent with hydrodynamic collective flow in d+Au. Perhaps more convincing evidence for hydrodynamic flow is given in Fig. 18b,c where both at RHIC in d+Au (b) and LHC in p+Pb (c), the characteristic π, p mass splitting for $v_2(p_T)$ seen in Au+Au is observed [53]. The splitting occurs because, for a given transverse collective expansion velocity β, protons have a larger $p_T = \gamma\beta m$ than pions.

6.1 v_2 in U+U collisions and constituent-quark participants

Because Uranium nuclei are prolate spheroids, there is the interesting possibility of large v_2 in body-to-body central collisions which have a significant eccentricity and almond shape (Fig. 19a). Based on the assumption that the $N_{\rm part}$, $N_{\rm coll}$ ansatz (Eq. 3) would describe the $dN_{\rm ch}/d\eta$ distribution in U+U collisions, it was predicted that for the highest $dN_{\rm ch}/d\eta$ (the most central collisions) the tip-to-tip configuration with much larger $N_{\rm coll}$ and small eccentricity (small v_2) would overtake the body-to-body configuration with large eccentricity corresponding to large v_2.

This led to two predictions: i) the tip-to-tip configuration would be selected by the most central collisions [54]; ii) these most central collisons would see a sharp decrease in v_2 with increasing $dN_{\rm ch}/d\eta$ [55, 56] called a cusp. This sharp decrease—represented by the bent line on the topmost U+U data (filled circles) in Fig. 19b (called a knee in Ref. [43])—is not observed. As discussed previously, this is because the $N_{\rm coll}$ term is not relevant for $dN_{\rm ch}/d\eta$ distributions, which also argues against the method proposed in Ref. [54] to select the tip-to-tip configuration.

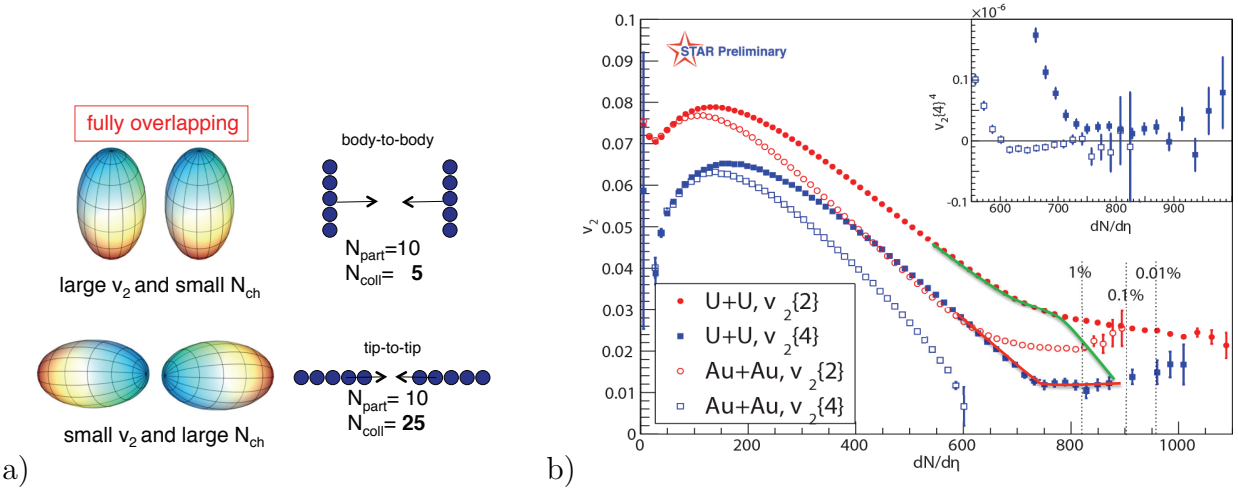

a) b)

Figure 19: (a) Body-to-body and tip-to-tip configurations in U+U collisions with zero impact parameter. The different relation of $N_{\rm part}$ to $N_{\rm coll}$ is sketched next to each configuration. (Modified drawing from Ref. [43]). (b) STAR measurements of v_2 in Au+Au and U+U at $\sqrt{s_{NN}} \approx 200$ GeV as a function of $dN_{\rm ch}/d\eta$ with upper percentiles of centrality for U+U indicated by vertical dashed lines [43].

7 RHIC Beam Energy Scan (BES)—in search of the critical point

In addition to discovering the QGP and measuring its properties, another objective of the RHIC physics program is to measure the phase diagram of nuclear matter and to determine the equation of state in the various phases and the characteristics of the phase transitions. Two of the many proposed phase diagrams of nuclear matter (e.g. see Ref. [57]) are shown in Fig. 20 together with the idealized trajectories of the evolution of the medium for Au+Au

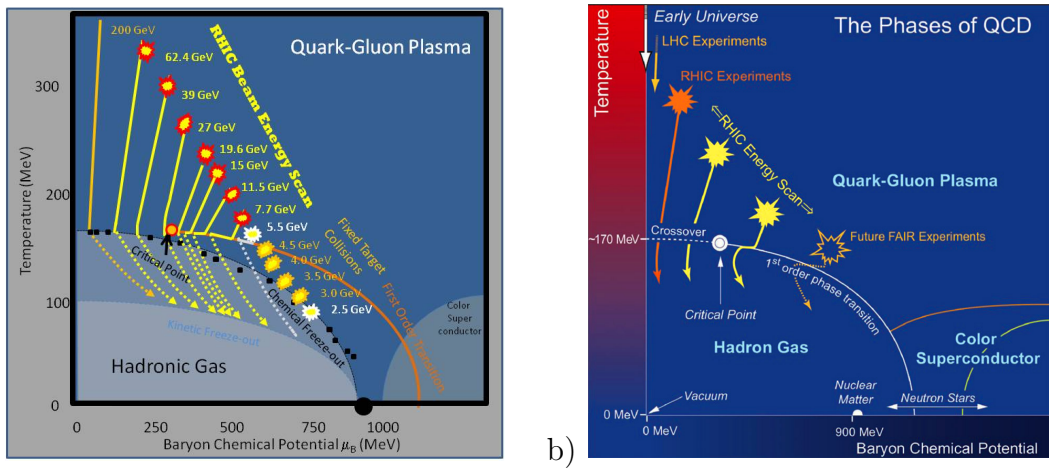

a) b)

Figure 20: Proposed phase diagrams for nuclear matter: Temperature, T, vs Baryon Chemical Potential, μ_B. a)STAR's idea in 2013 [58]; b) STAR's more cautious idea in 2014 [59].

collisions at the $\sqrt{s_{NN}}$ proposed for the Beam Energy Scan at RHIC to search for a QCD critical point. The bursts represent the hottest and densest stage of the medium when thermal equilibrium is reached shortly after the collision. The axes are the temperature T

vs. the baryon chemical potential μ_B. The temperature for the transition from the Quark Gluon Plasma (QGP) to a hadron gas is taken as 170 MeV for $\mu_B = 0$ and the phase boundary is predicted to be a smooth crossover down to a critical point below which the phase boundary becomes a first order phase transition.

In an equilibrated thermal medium, particles should follow a Boltzmann distribution in the local rest frame [60]

$$\frac{d^2\sigma}{dp_L p_T dp_T} = \frac{d^2\sigma}{dp_L m_T dm_T} \propto \frac{1}{e^{(E-\mu)/T} \pm 1} \sim e^{-(E-\mu)/T} \quad , \tag{6}$$

where $m_T = \sqrt{p_T^2 + m^2}$ and μ is a chemical potential. In fact, the ratios of particle abundances (which are dominated by low p_T particles) for central Au+Au collisions at RHIC, even for strange and multi-strange particles, are well described [61] by fits to a thermal distribution,

$$\frac{d^2\sigma}{dp_L p_T dp_T} \sim e^{-(E-\mu)/T} \rightarrow \frac{\bar{p}}{p} = \frac{e^{-(E+\mu_B)/T}}{e^{-(E-\mu_B)/T}} = e^{-(2\mu_B)/T} \quad , \tag{7}$$

with similar expressions for strange particles. μ_B (and μ_S) are chemical potentials associated with each conserved quantity: baryon number, μ_B, (and strangeness, μ_S). Thus it is simple and instructive to estimate the $\bar{p}/p$ ratio from Fig. 20a, near the arrow, where I read $T = 160$ MeV, $\mu_B = 300$ MeV, $\sqrt{s_{NN}} \approx 30$ GeV, which gives $\bar{p}/p \approx 0.02$. Since the $\bar{p}/p$ ratio vs $\sqrt{s_{NN}}$ will be an important issue later, it is not a good idea to get this important information from a sketch in a proposal but from measurements and the best analysis (Fig. 21). The results

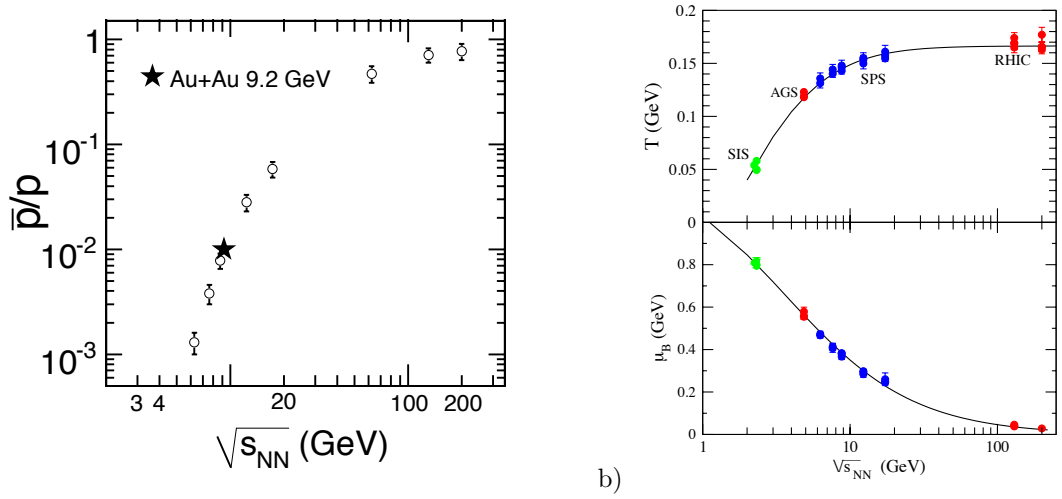

a) b)

Figure 21: (a) STAR measurements of $\bar{p}/p$ vs. $\sqrt{s_{NN}}$ [62]; b) Best accepted analysis of T and μ_B vs $\sqrt{s_{NN}}$ [63].

are: i) the correct $\bar{p}/p$ ratio at $\sqrt{s_{NN}} = 30$ GeV is ~ 0.12 from Fig. 21a; ii) this ratio also corresponds to the correct $\mu_b \approx 170$ MeV at $\sqrt{s_{NN}} = 30$ GeV from Fig. 21b. The lesson is: if it looks more like art than like science, be skeptical and look in refereed journals for the correct numbers.

7.1 A press release during ISSP 2011

On June 23, 2011, shortly before I was to present my 2011 lectures, a press release from LBL arrived claiming that "By comparing theory with data from STAR, Berkeley Lab scientists and their colleagues map phase changes in the QGP" [64]. Since I was going to criticize in my lectures what I considered to be a particularly egregious case of "physics by press release" in the year 2000 by CERN (see Ref. [9]), I felt that I was obliged to quickly absorb and present in my talk the physics behind this latest press release, hopefully a "Highlight from RHIC".

The subject is "Fluctuations of conserved quantities", in this case the net baryon distribution taken as $p - \bar{p}$. Since there can be no fluctuations of conserved quantities such as net charge or net baryon number in the full phase space, one has go to "locally conserved quantities" [65] in small rapidity intervals to detect a small fraction of the protons and anti-protons which then fluctuates, i.e. varies from event to event. The argument is that, e.g. the fluctuation of one charged particle in or out of the considered interval produces a larger mean square fluctuation of the net electric charge if the system is in the hadron gas phase with integral charges than for the QGP phase with fractional charges.

However, while there are excellent statistical mechanical arguments about the utility of fluctuations of conserved quantities such as net baryon number as a probe of a critical point [66], there were, in 2011, no adequate treatments of the mathematical statistics of the experimental measurements. There are also additional problems such as short-range rapidity correlations in A+A collisions between like-particles induced by Fermi or Bose quantum statistics that must be reckoned with (e.g. see Refs. [67, 68]).

Theoretical analyses tend to be made by a Taylor expansion of the free energy $F = -T \ln Z$ around the critical temperature T_c where Z is the partition function, or sum over states, which is of the form

$$Z \propto e^{-(E-\sum_i \mu_i Q_i)/kT} \tag{8}$$

and μ_i are chemical potentials associated with conserved charges Q_i [66]. The terms of the Taylor expansion, which are obtained by differentiation, are called susceptibilities, denoted χ. The only connection of this method to mathematical statistics is that the Cumulant generating function in mathematical statistics for a random variable x is also a Taylor expansion of the ln of an exponential:

$$g_x(t) = \ln \left\langle e^{tx} \right\rangle = \sum_{n=1}^{\infty} \kappa_n \frac{t^n}{n!} \qquad \kappa_m = \left. \frac{d^m g_x(t)}{dt^m} \right|_{t=0} \quad . \tag{9}$$

Thus, the susceptibilities are Cumulants in mathematical statistics terms, where, in general, the Cumulant κ_m represents the m^{th} central moment, $\mu_m \equiv \langle (x-\mu)^m \rangle$, with all m-fold combinations of the lower order moments subtracted, where $\mu \equiv \langle x \rangle$. For instance, $\kappa_2 = \langle (x-\mu)^2 \rangle \equiv \sigma^2$, $\kappa_3 = \langle (x-\mu)^3 \rangle$, $\kappa_4 = \langle (x-\mu)^4 \rangle - 3\kappa_2^2$, $\kappa_5 = \langle (x-\mu)^5 \rangle - 10\kappa_3\kappa_2$. Two so-called normalized or standardized Cumulants are common in this field, the skewness, $S \equiv \kappa_3/\sigma^3$ and the kurtosis, $\kappa \equiv \kappa_4/\sigma^4 = \langle (x-\mu)^4 \rangle / \sigma^4 - 3$.

A sample [69] of STAR measurements of the distribution of net-protons in Au+Au collisions in the small interval $0.4 \leq p_T \leq 0.8$ GeV/c, $|y| < 0.5$ for different $\sqrt{s_{NN}}$ is shown in Fig. 22a. The moments in the form $\kappa\sigma^2 = \kappa_4/\kappa_2$ are shown from a previous STAR publication [70] in Fig. 22b while a plot, alleged to be of this same data, presented in the Lattice

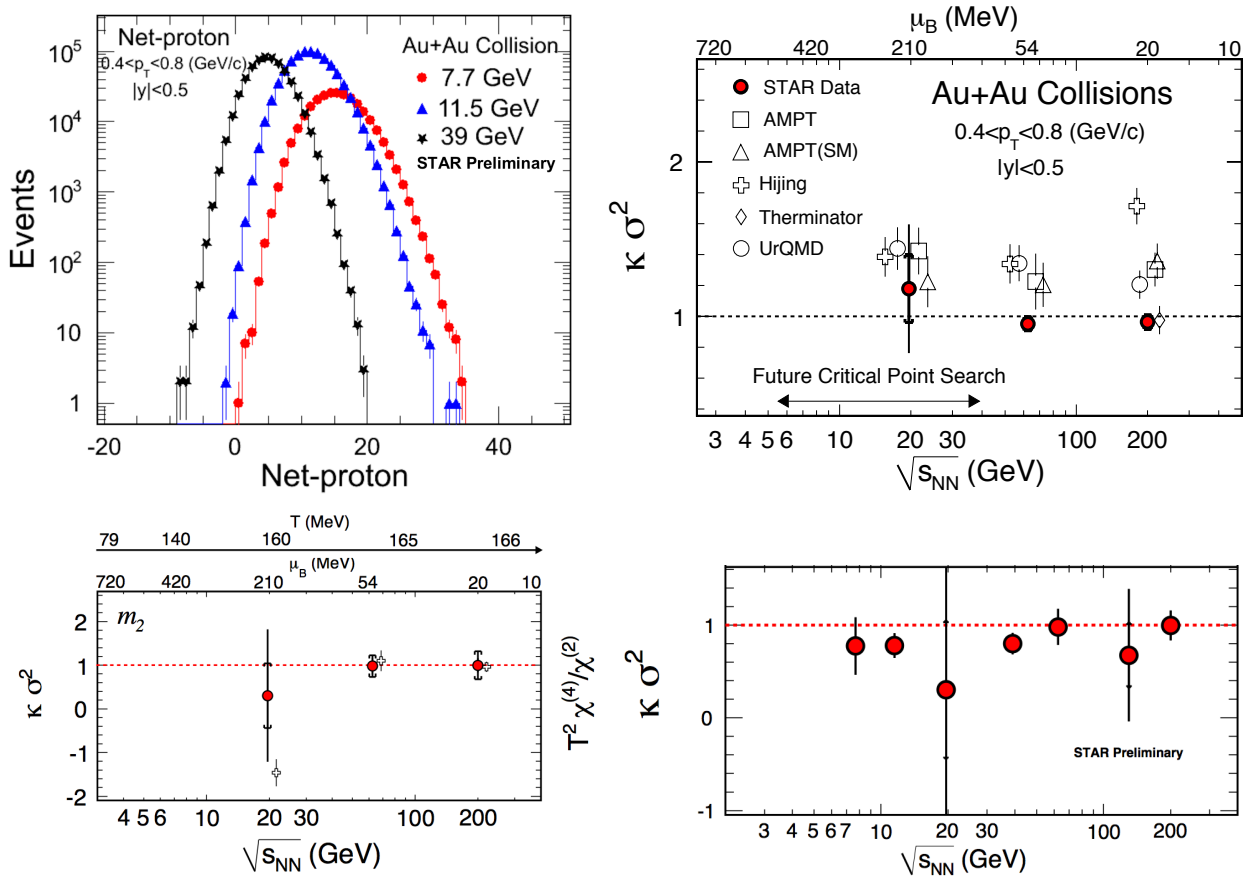

Figure 22: a) (top-left) STAR [69] distribution of event-by-event $p-\bar{p}$ at 3 values of $\sqrt{s_{NN}}$; b) (top-right) STAR published [70] measurements of $\kappa\sigma^2$; c) (bottom-left) Measurements from (b) as shown in Ref. [71] compared to the predicted ratio of susceptibilities (open crosses); d) (bottom-right) compilation [69] of STAR measurements of $\kappa\sigma^2$ for $p-\bar{p}$.

QCD theory publication that generated the press-release, is shown in Fig. 22c [71]; and a plot of the $\kappa\sigma^2$ from the data of Fig. 22c, combined with the results from Fig. 22b, is shown in Fig. 22d [69]. There are many interesting issues to be gleaned from Fig. 22.

The data point at 20 GeV in Fig. 22c is not the published one from (b), as stated in the caption [71], but the one from (d), which is different and with a much larger error. This, in my opinion, makes the data point look better compared to the predicted discontinuous value of $\kappa\sigma^2 = -1.5$ for the critical point at 20 GeV (open crosses) in contrast to the predictions of 1.0 for both 62.4 and 200 GeV. The published measurements in (b) together with the newer measurements in (d) are all consistent with $\kappa\sigma^2 = 1$; but clearly indicate the need for a better measurement at $\sqrt{s_{NN}} = 20$ GeV. Apart from these issues, the main problem of comparing Lattice QCD "data" to experimental measurements is that it is like comparing peaches to a fish, since the prediction is the result of derivatives of the log of the calculated partition function of an idealized system, which may have little bearing on what is measured using finite sized nuclei in an experiment with severe kinematic cuts. Maybe this is too harsh a judgement; but since this is the first such comparison (hence the press release), perhaps the situation will improve in the future. If a future measurement would show a significant huge discontinuity of $\kappa\sigma^2$ similar to the theoretical prediction at $\sqrt{s_{NN}} = 20$ GeV, then even I would admit that such a discovery would deserve a press release, maybe more!

7.1.1 If you know the distribution, you know all the moments and cumulants

When I first saw the measured distributions in Fig. 22a in 2011, my immediate reaction was that STAR should fit them to Negative Binomial distributions (NBD) so that they would know all the Cumulants. However, I subsequently realized that my favorite 3 distributions for integer random variables, namely, Poisson, Binomial, and Negative Binomial, are all defined only for positive integers (e.g. see Ref. [8] for details), while the number of net-protons on an event can be negative as well as positive, especially at higher c.m. energies. Thanks to Gary Westfall of STAR, in a paper presented at the Erice School of Nuclear Physics in 2012 [72], who found out that these three distributions fall into the class of "integer valued Lévy processes [73]" for which the Cumulants κ_j for the distribution $P(n-m)$ of the difference of samples from two such distributions, $P^+(n)$ and $P^-(m)$, with Cumulants κ_j^+ and κ_j^-, respectively, are [74, 73]:

$$\kappa_j = \kappa_j^+ + (-1)^j \kappa_j^- \qquad , \tag{10}$$

so long as the distributions are not 100% correlated. This result is the same as if the distributions $P^+(n)$ and $P^-(m)$ were statistically independent. The first four Cumulants of the Poisson, Binomial and Negative Binomial distributions are given in Table 2.

Table 2: Cumulants for Poisson, Binomial and Negative Binomial Distributions

Cumulant	Poisson	Binomial	Negative Binomial
$\kappa_1 = \mu$	μ	np	μ
$\kappa_2 = \mu_2 = \sigma^2$	μ	$\mu(1-p)$	$\mu(1+\mu/k)$
$\kappa_3 = \mu_3$	μ	$\sigma^2(1-2p)$	$\sigma^2(1+2\mu/k)$
$\kappa_4 = \mu_4 - 3\kappa_2^2$	μ	$\sigma^2(1-6p+6p^2)$	$\sigma^2(1+6\mu/k+6\mu^2/k^2)$
$S \equiv \kappa_3/\sigma^3$	$1/\sqrt{\mu}$	$(1-2p)/\sigma$	$(1+2\mu/k)/\sigma$
$\kappa \equiv \kappa_4/\kappa_2^2$	$1/\mu$	$(1-6p+6p^2)/\sigma^2$	$(1+6\mu/k+6\mu^2/k^2)/\sigma^2$
$S\sigma = \kappa_3/\kappa_2$	1	$(1-2p)$	$(1+2\mu/k)$
$\kappa\sigma^2 = \kappa_4/\kappa_2$	1	$(1-6p+6p^2)$	$(1+6\mu/k+6\mu^2/k^2)$

7.2 The latest measurements have appeared without a press release.

In the intervening period since 2011, the STAR collaboration has improved the preliminary measurements to publications and has improved the analysis by comparing to both Poisson and Negative Binomial distributions. Figure 23a [75] shows the STAR measurements of Cumulants of the net charge ($N^+ - N^-$) distributions from the "number of positive (N^+) and negative (N^-) charged particles within $|\eta| < 0.5$ and $0.2 < p_T < 2.0$ GeV/c on each event (after removing protons and antiprotons with $p_T < 400$ MeV/c) [75]". The corresponding Poisson and NBD Cumulants were calculated from the measured mean, μ, and variance, σ^2, of the N^+ and N^- distributions, respectively, and then calculated using Eq. 10. In contrast to Fig. 22, no non-monotonic behavior with $\sqrt{s_{NN}}$ is observed (or claimed) and the measurements of $S\sigma$ and $\kappa\sigma^2$ are all above the Poisson baseline. The $S\sigma$ measurements clearly favor the NBD.

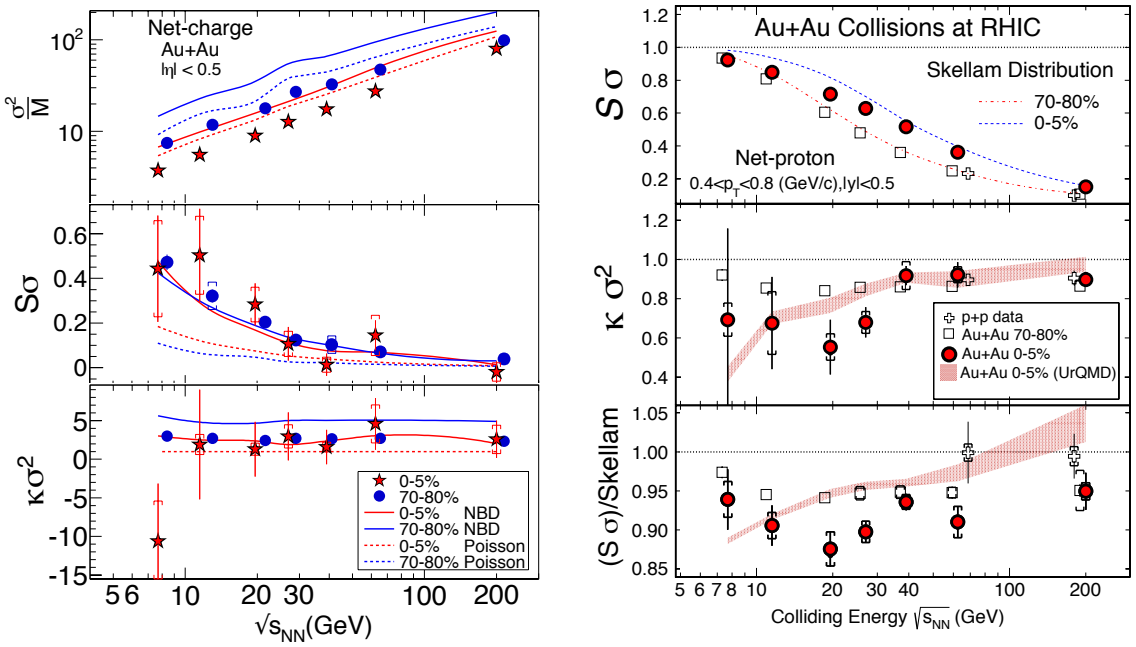

Figure 23: a) $\sqrt{s_{NN}}$ dependence of combinations of Cumulants in Au+Au (and p+p) from STAR: a) (left) net-charge Cumulants [75], where M is used to represent the mean, μ. b) (right) Cumulants of the $N_p - N_{\bar{p}}$ distributions [76], **where the error bars are statistical and the caps systematic errors**.

The situation is quite different for the net-proton ($N_p - N_{\bar{p}}$) Cumulants (Fig. 23b) [76] measured within $|y| < 0.5$ over the range $0.4 < p_T < 0.8$ GeV/c which covers roughly half the p_T spectrum. Here the measurements of $S\sigma$ and $\kappa\sigma^2$ are all below the Poisson baseline, denoted Skellam, which is the distribution of the difference between two Poissons and reflects "a system of totally uncorrelated, statistically random particle production"[76]. From Eq. 10 and Table 2 for a Poisson one can see that, for a Skellam, $S\sigma = \kappa_3/\kappa_2 = (\mu_p - \mu_{\bar{p}})/(\mu_p + \mu_{\bar{p}})$ which increases with decreasing $\sqrt{s_{NN}}$ because the $\bar{p}$ vanish ($\mu_{\bar{p}} = \langle N_{\bar{p}} \rangle \ll \mu_p$) so that the shape of the net distribution becomes dominated by the protons. This is easier to see in a plot of $\kappa\sigma^2$ vs μ_B with $\sqrt{s_{NN}}$ indicated (Fig. 24a) [59] which shows clearly that $\kappa\sigma^2$ starts dropping for $\sqrt{s_{NN}} < 39$ GeV where the $\bar{p}/p$ ratio drops below ~ 0.3 (recall Fig. 21).

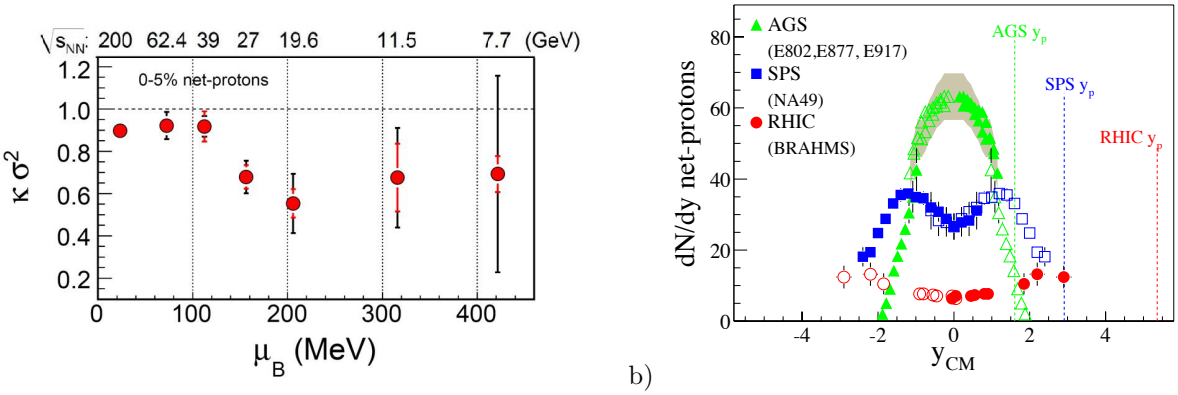

a) b)

Figure 24: (a)(left) $\kappa\sigma^2$ vs. $\sqrt{s_{NN}}$ and μ_B [59]; b) (right) $(dN_p/dy - dN_{\bar{p}}/dy)$ for top 5% centrality at AGS (Au+Au, $\sqrt{s_{NN}}$ =4.9 GeV), SPS (Pb+Pb, $\sqrt{s_{NN}}$ =17.2 GeV) and RHIC(Au+Au, $\sqrt{s_{NN}}$ =200 GeV), beam rapidity in c.m. system $y_p = 1.6, 2.9, 5.4$ [77].

The errors are still too large to determine whether or not $\kappa\sigma^2$ stays constant below $\sqrt{s_{NN}}$ =19.6 GeV but are sufficient to clearly rule out the value of $\kappa\sigma^2 = -1.5$ at $\sqrt{s_{NN}} \approx 20$ GeV predicted in Fig. 22 [71] which created the fuss in 2011. It is also important to point out that in addition to the vanishing of the anti-protons, the physics of the protons at mid-rapidity changes dramatically—the protons are no longer produced particles, which would conserve $N_p - N_{\bar{p}}$, but are the participants and fragments from the colliding nuclei which move to mid-rapidity and eventially stop as $\sqrt{s_{NN}}$ is reduced from 200, to 17.2 to 4.9 GeV (Fig. 24b) [77]. All these results indicate that the search for a QCD critical point at RHIC in the Beam Energy Scan (BES) in 2018-19 may not be as straightforward as originally assumed.

8 Jet quenching, RHIC's main claim to fame

The gold-plated signature for the QGP since 1986 [78] has been the suppression of J/Ψ because the color potential between $c, \bar{c}$ quarks would be screened (Debye screening) by all the free color charges in the medium so that the $c, \bar{c}$ would not be able to bind to form the J/Ψ. In fact the PHENIX experiment at RHIC was specifically designed to detect the J/Ψ at mid-rapidity at rest or with very low p_T (where the screening effect would be the largest) via the decay $J/\Psi \rightarrow e^+ + e^-$. J/Ψ suppression was reportedly observed several times at the CERN SpS fixed target heavy ion program starting with NA38 in O+U collisions in 1989 [79] but was plagued with many problems. The principal physics problem is that the J/Ψ does not follow the standard hard-scattering pointlike scaling in A+B collisions, $\sigma_{AB}^{J/\Psi} = (A \cdot B)^{\alpha} \cdot \sigma_{NN}^{J/\Psi}$ with $\alpha \equiv 1$, but is suppressed in cold nuclear matter (CNM) in p+A and A+B collisions, with $\alpha \approx 0.91$. Thus, the ultimate discovery by NA50 in Pb+Pb collisions at $\sqrt{s_{NN}}$ =17.2 GeV [80] in 1996–1998 was called "anomalous suppression" because it was below the CNM cross section dependence which was itself well below the hard-scattering pointlike scaling.

In 1998 at the QCD workshop in Paris [81], I found what I thought was a cleaner signal of the QGP when Rolf Baier asked me whether jets could be measured in Au+Au collisions because he had made studies in pQCD [82] of the energy loss of partons, produced by hard-scattering "with their color charge fully exposed", in traversing a medium "with a large density of similarly exposed color charges". The conclusion was that "Numerical estimates of the loss suggest that it may be significantly greater in hot matter than in cold. *This makes the magnitude of the radiative energy loss a remarkable signal for QGP formation*" [82]. In addition to being a probe of the QGP the fully exposed color charges allow the study of parton-scattering with $Q^2 \ll 1 - 5$ (GeV/c)^2 in the medium where new collective QCD effects may possibly be observed.

Because the expected energy in a typical jet cone $R = \sqrt{(\Delta\eta)^2 + (\Delta\phi)^2}$ in central Au+Au collisions at $\sqrt{s_{NN}}$ =200 GeV would be $\pi R^2 \times 1/2\pi \times d\mathrm{E}_T/d\eta = R^2/2 \times d\mathrm{E}_T/d\eta \sim 350$ GeV for $R = 1$, where the kinematic limit is 100 GeV, I said (and wrote [81]) that jets can not be reconstructed in Au+Au central collisions at RHIC—still correct after 16 years. On the other hand, hard-scattering was discovered in $p + p$ collisions at the CERN-ISR in 1972 with single particle and two-particle correlations, while jets had a long learning curve from 1977–1982 with a notorious false claim (e.g. see Refs. [8, 9]), so I said (and wrote [81]) that we should use single and two-particle measurements—which we did and it WORKED! The present solution for jets in A+A collisions (LHC 2010 and RHIC c.2014) is to take smaller cones, with 56 GeV in $R = 0.4$, 32 GeV in $R = 0.3$, 14 GeV in $R = 0.2$ at RHIC.

8.1 Jet quenching at RHIC — Suppression of high p_T particles

The discovery at RHIC [83] that π^0's produced at large transverse momenta are suppressed in central Au+Au collisions by a factor of ~ 5 compared to pointlike scaling from p+p collisions is arguably *the* major discovery in Relativistic Heavy Ion Physics. For π^0 (Fig. 25a) [84] the hard-scattering in p+p collisions is indicated by the power law behavior p_T^{-n} for the invariant cross section, $Ed^3\sigma/dp^3$, with $n = 8.1 \pm 0.1$ for $p_T \geq 3$ GeV/c. The Au+Au data at a given p_T can be characterized either as shifted lower in p_T by $\delta p_T'$ from the pointlike scaled p+p data at $p_T' = p_T + \delta p_T'$, or shifted down in magnitude, i.e. suppressed. In Fig. 25b, the suppression of the many identified particles measured by PHENIX at RHIC is presented as the Nuclear Modification Factor, $R_{AA}(p_T)$, the ratio of the yield of e.g. π per central Au+Au

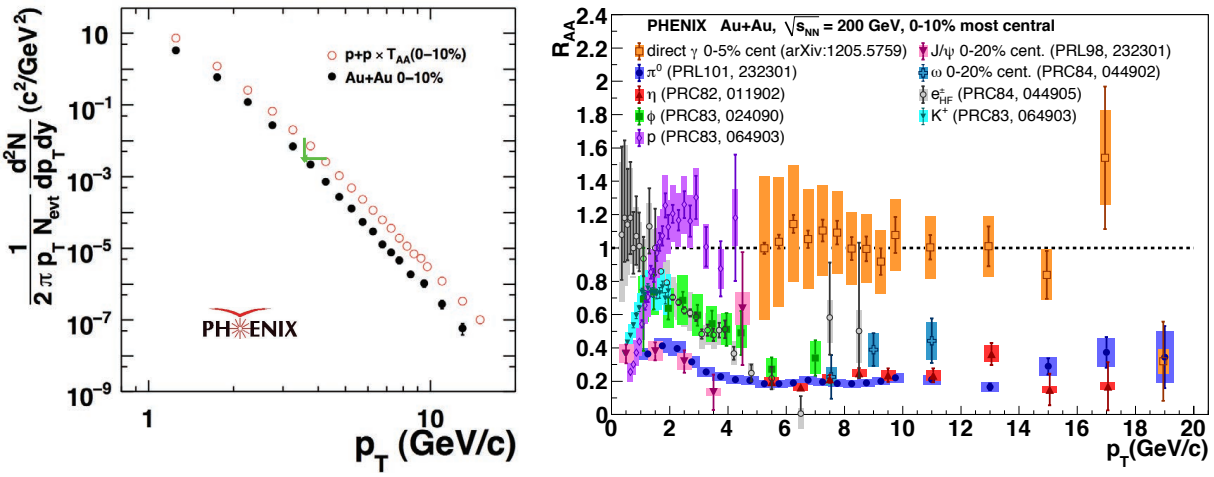

Figure 25: a) (left) Log-log plot of invariant yield of π^0 at $\sqrt{s_{NN}} = 200$ GeV as a function of transverse momentum p_T in p+p collisions multiplied by $\langle T_{AA}\rangle$ for Au+Au central (0–10%) collisions compared to the Au+Au measurement [84]. Vertical arrow is for $R_{AA}(p_T)$, horizontal arrow for $\delta p_T'$. b) (right) $R_{AA}(p_T)$ for all identified particles so far measured by PHENIX in Au+Au central collisions at $\sqrt{s_{NN}} = 200$ GeV.

collision (upper 10%-ile of observed multiplicity) to the pointlike-scaled p+p cross section at the same p_T, where $\langle T_{AA}\rangle$ is the average overlap integral of the nuclear thickness functions:

$$R_{AA}(p_T) = \frac{(1/N_{AA})\ d^2N_{AA}^{\pi}/dp_T dy}{\langle T_{AA}\rangle\ \ d^2\sigma_{pp}^{\pi}/dp_T dy} \quad . \tag{11}$$

The striking differences of $R_{AA}(p_T)$ in central Au+Au collisions for the many particles measured by PHENIX (Fig. 25b) illustrates the importance of particle identification for understanding the physics of the medium produced at RHIC. Most notable are: the equal suppression of π^0 and η mesons by a constant factor of 5 ($R_{AA} = 0.2$) for $4 \leq p_T \leq 15$ GeV/c, with suggestion of an increase in R_{AA} for $p_T > 15$ GeV/c; the equality of suppression of direct-single $e^{\pm}$ (from heavy quark (c, b) decay) and π^0 at $p_T \gtrsim 5$ GeV/c; the non-suppression of direct-γ for $p_T \geq 4$ GeV/c; the exponential rise of R_{AA} of direct-γ for $p_T < 2$ GeV/c [85], which is totally and dramatically different from all other particles and attributed to thermal photon production by many authors (e.g. see citations in Ref. [85]). For $p_T \gtrsim 4$ GeV/c, the hard-scattering region, the fact that all hadrons are suppressed, but direct-γ are not suppressed, indicates that suppression is a medium effect on outgoing color-charged partons likely due to energy loss by coherent Landau-Pomeranchuk-Migdal radiation of gluons, predicted in pQCD [82], which is sensitive to properties of the medium.

One nice advantage that hard-scattering and high p_T suppression have as a QGP probe compared to J/Ψ suppression is that although there is a CNM effect, it is an enhancment rather than a suppression; and as far as is known, the enhancement, historically called the Cronin effect [86], only occurs for baryons and not mesons at RHIC energies. Figure 26a

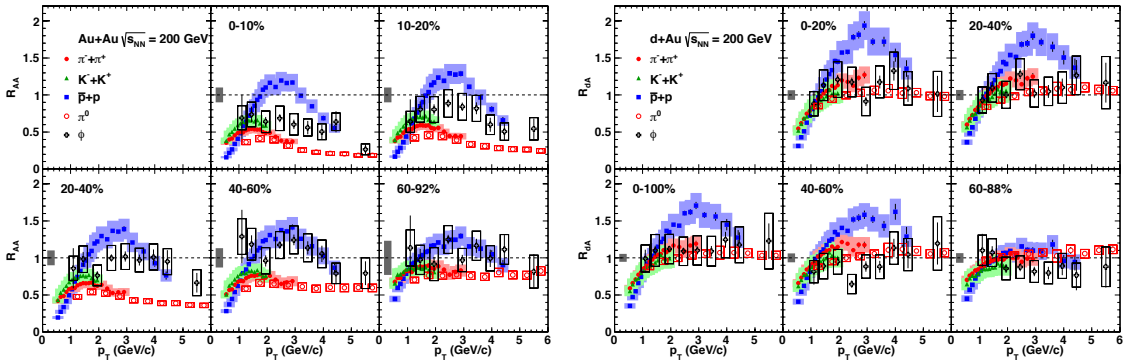

Figure 26: Measurements of R_{AA} of identified particles $\pi^{\pm}, K^{\pm}, p^{\pm}, \pi^0, \phi$ as a function p_T and centrality at $\sqrt{s_{NN}} = 200$ GeV [87]: a) (left) Au+Au; b) (right) d+Au.

shows R_{AA} in Au+Au for protons and mesons in the range $0.5 < p_T < 6.0$ GeV/c, where, in central collisions (0-10%), all the mesons are suppressed for $p_T > 2$ GeV/c while the protons are enhanced for $2 < p_T < 4$ GeV/c and then become suppressed at larger p_T. The d+Au results in Fig. 26b show no CNM effect for the mesons, $R_{AA} \approx 1$ out to $p_T = 6$ GeV/c; while the protons show a huge enhancement (Cronin effect) in all centralities except for the most peripheral (60-88%). At present, there is no explanation of the proton enhancement in either Au+Au or d+Au collisions, so π^0 and η are the favored hard-probes.

8.2 $\delta p'_T/p'_T$, the fractional shift in the p'_T spectrum

After more than a decade of using the ratio R_{AA}, we are now paying more attention to $\delta p'_T/p'_T$, the fractional shift of the p'_T spectrum, as an indicator of energy loss in the QGP Fig. 27 [88]. For a constant fractional energy loss, which is true at RHIC in the range $6 < p_T < 12$ GeV/c (as shown in Fig. 25a where the p+p reference and Au+Au measurement are parallel on a log-log plot) there is a simple relationship between R_{AA}, $\delta p'_T/p'_T$ and n, the power in the invariant p_T spectra:

$$R_{AA}(p'_T) = R_{AA}(p_T) = (1 - \delta p_T/p_T)^{n-2} \quad . \tag{12}$$

Using $\delta p_T/p_T$ is important for comparison to the LHC measurements where the power is $n \approx 6$ compared to $n = 8.1$ at RHIC, so that the same R_{AA} does not mean the same $\delta p_T/p_T$. Strictly $\delta p_T/p_T$ is not a measure of the parton energy loss in the QGP but is used as a proxy. Figure 27a shows that $\delta p_T/p_T$ at $p_T = 7$ GeV/c for RHIC and LHC both increase monotonically with centrality ($N_{\rm part}$) but is a factor of 2 to 1.4 larger at LHC, depending on centrality, a likely indication of a hotter and/or denser medium. Figure 27b attempts to determine whether $\delta p_T/p_T$ is a universal function of the charged particle density, $dN_{\rm ch}/d\eta$ at both RHIC and LHC. The dependence is not quite universal. A fit of $\delta p_T/p_T \propto (dN_{\rm ch}/d\eta)^{\alpha}$ gives $\alpha \approx 0.35$ at LHC and 0.55 at RHIC, although the data at $\sqrt{s_{NN}} = 200$ GeV and 2.76 TeV do appear to merge for $(dN_{\rm ch}/d\eta) \geq 300$. Hopefully, measurements of $\delta p_T/p_T$ will eventually lead to the determination of dE/dx of partons in the QGP.

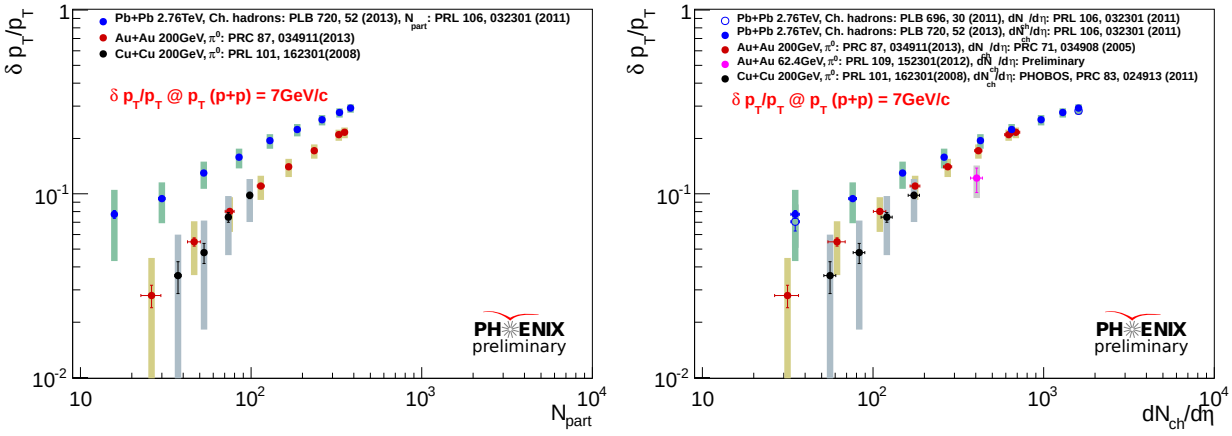

Figure 27: Plots from PHENIX [88] of $\delta p'_T/p'_T$ at $p'_T \equiv p_T(p+p) = 7$ GeV for π^0 (RHIC) and charged hadrons (LHC): a) as a function of centrality ($N_{\rm part}$), b) as a function of $dN_{\rm ch}/d\eta$.

8.3 At last: jet measurements in Au+Au at RHIC in 2014?

Some interesting new jet measurements in A+A collisions at RHIC were presented at Quark Matter 2014 in a plenary review talk on jets by Yen-Jie Lee who works on CMS [89]. Figure 28 shows that the STAR charged jets in a cone with $R = 0.2$ have much less suppression ($R_{AA} \gg 0.3$) than π^0 ($0.2 \le R_{AA} \le 0.3$) in the range $10 < p_T < 20$ GeV.

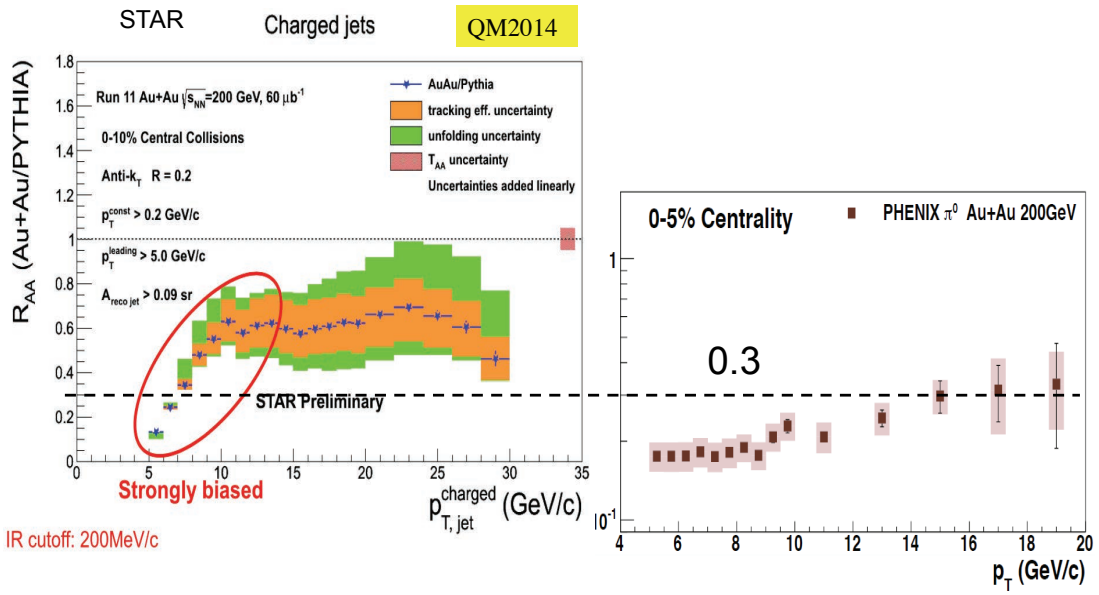

Figure 28: a) (left) STAR R_{AA} for charged jets at $\sqrt{s_{NN}}$ =200 GeV in central Au+Au collisions (see details in legend) compared to b) R_{AA} for PHENIX π^0. The dashed line at 0.3 is the maximum R_{AA} for π^0 in this p_T range.

This is quite different from jets at the LHC (Fig. 29) which have comparable or smaller R_{AA} than charged particles from jet fragmentation in the range $30 < p_T < 100$ GeV. Note that the γ, W and Z^0 bosons in Fig. 29b which are not coupled to color are not suppressed.

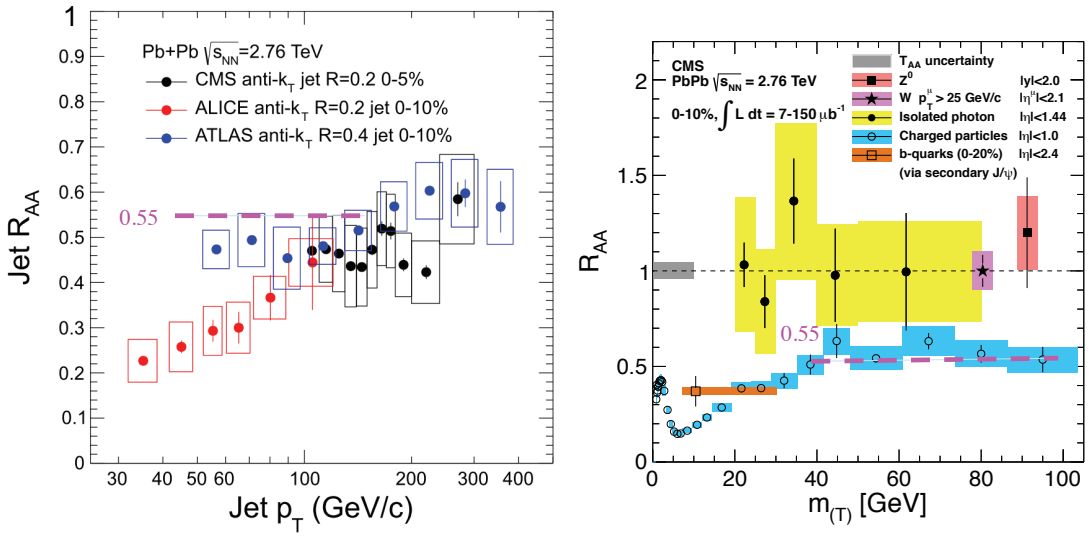

Figure 29: a) (left) R_{AA} for jets at $\sqrt{s_{NN}}$ =2.76 GeV by CMS and ALICE compared to b) CMS R_{AA} for charged hadrons ($R_{AA} \approx 0.55$), b-quarks and 3 favorite Electro-Weak Bosons [89].

For STAR, the disagreement of the jet and single particle R_{AA} gets worse as the jet cone is increased from R=0.2 to 0.3 to 0.4 (Fig. 30). Some people would say that this is great because all the jet fragments and/or any energy lost in the QGP by the originating parton have been captured in the R=0.4 cone. Skeptics like myself can hardly wait to see what happens when the jet cone is further increased. After 14 runs at RHIC, the jet learning curve in Au+Au central collisions still has a way to go.

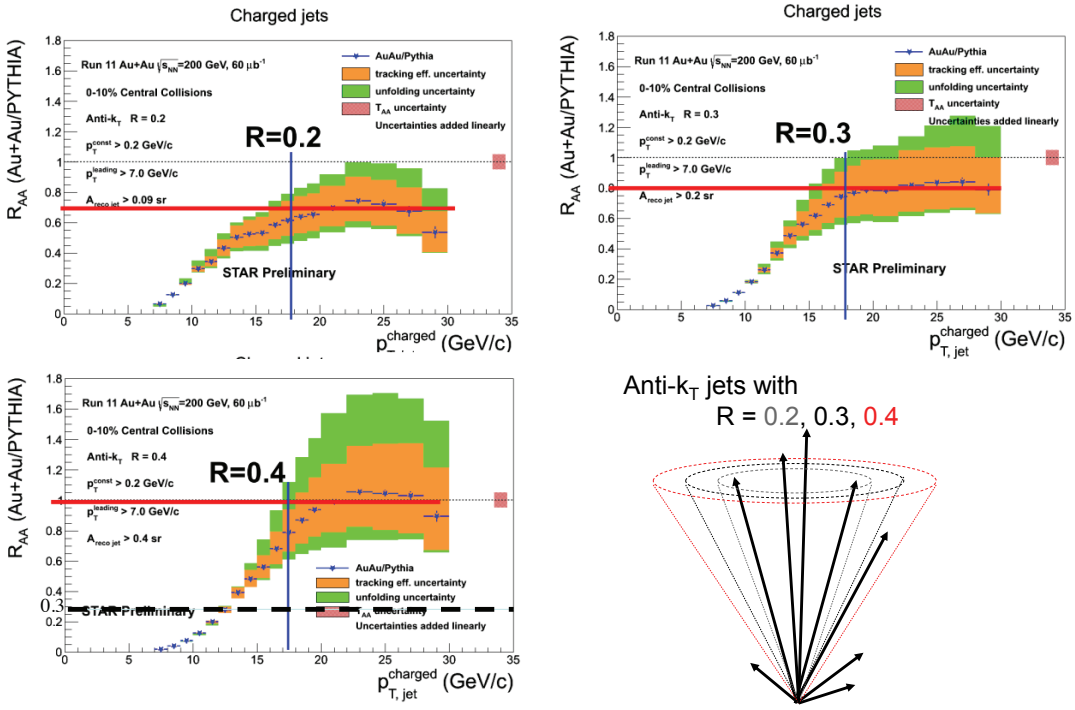

Figure 30: STAR R_{AA} for charged jets at $\sqrt{s_{NN}}$ =200 GeV in central Au+Au collisions for 3 different jet cones with $R = 0.2, 0.3, 0.4$ (see details in legend and sketch) [89].

The good news for the future is that a new detector, now called sPHENIX, to find jets by the more traditional method using hadron calorimetry has been proposed, is moving along on the approval process and is on the schedule at RHIC (Fig. 5b) for comissioning and full

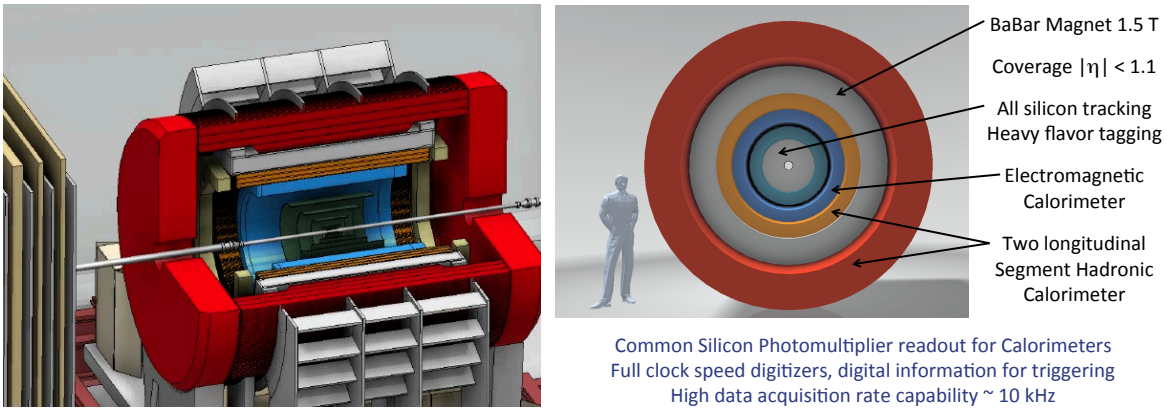

Figure 31: a)(left) new detector in place of PHENIX; b) (right) beam's eye view with details [90].

installation in the PHENIX IR in 2019–20. It is based on the (made in Italy) BABAR superconducting solenoid from SLAC which became available when the B-factory in Italy was unfortunately cancelled. Design work is moving along quickly (Fig. 31) so now is the optimum time for new collaborators to join.

References

[1] See `http://bnlcompetition.science.energy.gov` for details.

[2] *Building for Discovery, Strategic Plan for U.S. Particle Physics in the Global Context*, `http://science.energy.gov/~/media/hep/hepap/pdf/May%202014/FINAL_P5_Report_053014.pdf`

[3] Stanley Wojcicki, Rev. Accl. Sci. Tech. *The Supercollider: The Pre-Texas Days*, **01** (2008) 259; *The Texas Days*, **02** (2009) 265.

[4] PHENIX Collaboration (S. S. Adler *et al.*), Phys. Rev. C**89** (2014) 044905.

[5] PHENIX Collaboration (K. Adcox *et al.*), Nucl. Phys. A**757** (2005) 184–283.

[6] M. Harrison, T. Ludlam and S. Qzaki (eds.), *The Relativistic Heavy Ion Collider Project: RHIC and its Detectors*, Nucl. Instrum. Methods A**499** (2003) 235–880.

[7] M. J. Tannenbaum, Int. J. Mod. Phys. A**26** (2011) 5299-5335, arXiv:1406.0830.

[8] Jan Rak and Michael J. Tannenbaum, *High p_T Physics in the Heavy Ion Era*, (Cambridge University Press, 2013).

[9] M. J. Tannenbaum, Int. J. Mod. Phys. A**29** (2014) 1430017, arXiv:1406.1100.

[10] W. Busza, *et al.*, Phys. Rev. Lett. **34** (1975) 836–839.

[11] J. E. Elias, *et al.*, Phys. Rev. D**22** (1980) 13–35.

[12] C. Halliwell, *et al.*, Phys. Rev. Lett. **39** (1977) 1499–1502.

[13] S. Frankel, Phys. Rev. C**48** (1993) R2170.

[14] A. Białas, M. Bleszyński, W. Czyż, Nucl. Phys. B**111** (1976) 461–476.

[15] A. Bialas, W. Czyz, and L. Lesniak, Phys. Rev. D**25** (1982) 2328.

[16] W. J. Willis, Report CRISP-72-15, BNL-16841, Upton, NY, 1972.

[17] J. D. Bjorken, Phys. Rev. D**8** (1973) 4098.

[18] BCMOR Collaboration, (A.L.S. Angelis *et al.*), Phys. Lett. B**141** (1984) 140.

[19] BCMOR Collaboration, (Michael J. Tannenbaum *et al.*), Lect. Notes Phys. **221** (1985) 174.

[20] AFS Collaboration, (Bruce Callen *et al.*), Lect. Notes Phys. **221** (1985) 133.

[21] T. Ochiai, Z. Phys. C**35** (1987) 209.

[22] CMOR Collaboration, (A.L.S. Angelis *et al.*), Nucl. Phys. B**244** (1984) 1.

[23] L. DiLella, Ann. Rev. Nucl. Part. Sci. **35** (1985) 107.

[24] PHENIX Collaboration, (K. Adcox *et al.*), Phys. Rev. Lett. **86** (2001) 3500.

[25] X.-N. Wang and M. Gyulassy, Phys. Rev. Lett. **86** (2001) 3496.

[26] ALICE Collaboration, (K. Aamodt *et al.*), Phys. Rev. Lett. **106** (2011) 032301.

[27] PHENIX Collaboration, (J. T. Mitchell *et al.*), PoS CPOD2013 (2013) 003.

[28] S. Eremin and S. Voloshin, Phys. Rev. C**67** (2003) 064905.

[29] M. Gell-Mann, Phys. Lett. **8** (1964) 214.

[30] E. V. Shuryak, Nucl. Phys. B**203** (1982) 116.

[31] M. Breidenbach *et al.*, Phys. Rev. Lett. **23** (1969) 935.

[32] T. Kalaydzhyan and E. Shuryak, Phys. Rev. C**90** (2014) 014901.

[33] R. Hofstadter, F. Bumiller, and M. R. Yerian, Rev. Mod. Phys. **30** (1958) 482.

[34] PHENIX Collaboration, (S. S. Adler *et al.*), Phys. Rev. D**76** (2007) 051006(R).

[35] ATLAS Collaboration, (G. Aad *et al.*), Phys. Lett. B**707** (2012) 330.

[36] ALICE Collaboration, (B. Abelev *et al.*) Phys. Rev. C**88** (2013) 044909.

[37] PHOBOS Collaboration, (B. B. Back *et al.*), Phys. Rev. C**70** (2004) 021902(R).

[38] L. Zhou and G. S. F. Stephans, Phys. Rev. C**90** (2014) 014902.

[39] PHOBOS Collaboration, (B. Alver *et al.*), Phys. Rev. C**83** (2011) 024913.

[40] H. Bialkowska, Acta Phys. Polon. **B37** (2006) 3415.

[41] PHOBOS Collaboration (B. B. Back, *et al.*), Phys. Rev. C**74** (2006) 021901(R).

[42] M. Basile, ... A. Zichichi, *et al.*, Phys. Lett. B**95** (1980) 311–312.

[43] STAR Collaboration (Hui Wang *et al.*), Flow measurements and selection of body-body and tip-tip enhanced samples in U+U collisions, presented at *Quark Matter 2014*, Darmstadt, Germany, May 19, 2014. Also see http://dx.doi.org/10.1016/j.nuclphysa.2014.09.111.

[44] H. A. Gustafsson, *et al.*, Phys. Rev. Lett. **52** (1984) 1590.

[45] J.-Y. Ollitrault, Phys. Rev. D**46** (1992) 229–245, Nucl. Phys. A**638** (1998) 195c–206c.

[46] PHENIX Collaboration (M. Kaneta *et al.*), J. Phys. G**30** (2004) S1217–S1220.

[47] U. Heinz and R. Snellings, Ann. Rev. Nucl. Part. Sci. **63** (2013) 123.

[48] S. A. Voloshin, A. M. Poskanzer and R. Snellings, arXiv:0809.2949v2.

[49] FOPI Collaboration (A. Andronic *et al.*), Nucl. Phys. A**679** (2001) 765–792.

[50] M. Nasim, L. Kumar, P. K. Netraknti and B. Mohanty, Phys. Rev. C**82** (2010) 054908.

[51] D. Teaney, Phys. Rev. C**68** (2003) 034913.

[52] P. K. Kovtun, D. T. Son, and A. O. Starinets, Phys. Rev. Lett. **94** (2005) 111601.

[53] PHENIX Collaboration (A. Adare *et al.*), arXiv:1404.7461.

[54] A. Kuhlman and U. Heinz, Phys. Rev. C**72** (2005) 037901.

[55] P. Filip, R. Lecnicky, H. Masui and N. Xu, Phys. Rev. C**80** (2009) 054903.

[56] S. A. Voloshin, Phys. Rev. Lett. **105** (2010) 172301.

[57] J. M. Pawlowski, Equation of state and phase diagram of strongly interacting matter, presented at *Quark Matter 2014*, Darmstadt, Germany, May 22, 2014.

[58] STAR Collaboration, *RHIC Beam Use Request For Runs 14 and 15*, May 28, 2013. https://indico.bnl.gov/getFile.py/access?resId=0&materialId=2&confId=632

[59] STAR Collaboration, *Studying the Phase Diagram of QCD Matter at RHIC*, June 1, 2014. https://indico.bnl.gov/getFile.py/access?resId=0&materialId=2&confId=764

[60] F. Cooper and G. Frye, Phys. Rev. D**10** (1974) 186–189.

[61] STAR Collaboration, (J. Adams *et al.*), Nucl. Phys. A**757** (2005) 102183.

[62] STAR Collaboration, (B. I. Abelev *et al.*), Phys. Rev. C**81** (2010) 024911.

[63] J. Cleymans, H. Oeschler, K. Redlich and S. Wheaton, Acta Phys. Polon. Supp. **3** (2010) 533–538, arXiv:0911.0526.

[64] http://newscenter.lbl.gov/news-releases/2011/06/23/when-matter-melts/.

[65] M. Asakawa, U. Heinz, and B. Müller, Phys. Rev. Lett. **85** (2000) 2072.

[66] e.g. see V. Koch, PoS(CFRNC2006)008

[67] W. A. Zajc *et al.*, Phys. Rev. C**29** (1984) 2173.

[68] M. J. Tannenbaum, Phys. Lett. B**347** (1995) 431.

[69] Presentation by T. J. Tarnowsky at *Quark Matter 2011*, Annecy, France, May 23, 2011; STAR Collaboration (T. J. Tarnowsky *et al.*), J. Phys. G**38** (2011) 124054.

[70] STAR Collaboration (M. M. Aggarwal *et al.*), Phys. Rev. Lett. **105** (2010) 022302.

[71] S. Gupta, X. Luo, B. Mohanty, H. G. Ritter and N. Xu, Science **332** (2011) 1525.

[72] STAR Collaboration (G. Westfall *et al.*), Search for the QCD Critical Point, *International School of Nuclear Physics, 33rd Course* Erice, Sicily, Italy 16–24 September 2011.

[73] O. E. Barndorff-Nielsen, D. G. Pollard and N. Shephard, Quant. Finance **12** (2012) 587–605.

[74] T. J. Tarnowsky and G. D. Westfall, Phys. Lett. B**724** (2013) 51.

[75] STAR Collaboration (L. Adamczyk *et al.*), Phys. Rev. Lett. **113** (2014) 092301.

[76] STAR Collaboration (L. Adamczyk *et al.*), Phys. Rev. Lett. **112** (2014) 032302.

[77] BRAHMS Collaboration (I. G. Bearden *et al.*), Phys. Rev. Lett. **93** (2004) 102301.

[78] T. Matsui and H. Satz, Phys. Lett. B**178** (1986) 416.

[79] NA38 Collaboration (C. Baglin *et al.*), Phys. Lett. B**220** (1989) 471; L. Kluberg, Nucl. Phys. A**488** (1988) 613c.

[80] NA50 Collaboration (M. Gonin *et al.*), Nucl. Phys. A**610** (1996) 404c.

[81] R. Baier, M. J. Tannenbaum in *Proc. IV Workshop on Quantum Chromodynamics*, Paris, France, 1–6 June 1998, eds. H. M. Fried and B. Müller (World Scientific,1999).

[82] See R. Baier, D. Schiff and B. G. Zakharov, Ann. Rev. Nucl. Part. Sci. **50** (2000) 37–69, and references therein.

[83] PHENIX Collaboration (K. Adcox *et al.*), Phys. Rev. Lett. **88** (2002) 022301.

[84] PHENIX Collaboration (S. S. Adler *et al.*), Phys. Rev. C**76** (2007) 034904.

[85] PHENIX Collaboration (A. Adare, *et al.*), Phys. Rev. Lett. **104** (2010) 132301.

[86] J. W. Cronin *et al.*, Phys. Rev. D**11** (1975) 3105.

[87] PHENIX Collaboration (A. Adare, *et al.*), Phys. Rev. C**88** (2013) 024906.

[88] Presentation by T. Sakaguchi at *10th International Workshop on High p_T Physics in the RHIC/LHC era*, Nantes, France, 9–12 September 2014.

[89] Yen-Jie Lee, Experimental results on jets in ultra-relativistic nuclear collisions, presented at *Quark Matter 2014*, Darmstadt, Germany, May 23, 2014.

[90] PHENIX Collaboration (J. Nagle, *et al.*) sPHENIX Science Overview, presented at *Department of Energy sPHENIX Science Review*, BNL, Upton, NY, USA, July 1, 2014.